Electronic Structure and Optical Properties of Amorphous Semiconductors

Chapter · January 2007

DOI: 10.1007/BFb0107701

1 author:

Bernhard Kramer
University of Hamburg
306 PUBLICATIONS **8,488** CITATIONS

Festkörperprobleme XII (1972)

Electronic Structure and Optical Properties of Amorphous Semiconductors

Bernhard Kramer

Institut für Physik der Universität Dortmund

Summary: The theory of the electronic density of states and the optical absorption of structurally disordered solids is briefly reviewed. Two complementary descriptions of the problem are considered: The tight binding approach allows for the evaluation of the general properties of the electronic spectrum. The nearly free electron approximation yields a method for calculating the electronic properties of real amorphous systems. The structure dependence of the electronic density of states and the optical absorption spectrum of covalent bonded semiconductors is investigated. Results are presented for tetrahedrally bonded semiconductors and the chain structures selenium and tellurium. A comparison between the results of different theoretical approaches and experimental data is performed.

Zusammenfassung: Die Theorie der elektronischen Zustandsdichte und der optischen Absorption amorpher Festkörper mit Nahordnung wird kurz beschrieben. Zwei komplementäre Aspekte des Problems werden näher betrachtet: Eine Tight Binding Näherung, mit deren Hilfe man sich auf einfache Weise einen allgemeinen Überblick über das Energiespektrum der Elektronen verschaffen kann und die Näherung fast freier Elektronen, die es erlaubt, eine Methode zur Berechnung der elektronischen Eigenschaften realer amorpher Systeme herzuleiten. Die Strukturabhängigkeit der elektronischen Zustandsdichte und der optischen Absorption kovalenter Halbleiter wird untersucht. Ergebnisse für verschiedene tetraedrisch gebundene Halbleiter sowie die Kettenstrukturen Selen und Tellur werden diskutiert. Ein Vergleich mit experimentellen Resultaten wird durchgeführt.

Introduction

The electronic properties of ideal crystals are well understood. Unfortunately, in reality crystalline solids contain always a certain amount of impurities and structural defects. If the density of these perturbations of the perfect order is only small, one can still use the crystalline approximation for a theoretical description of the physical phenomena. With increasing rate of perturbation, however, the limitations of the crystalline approximation become more and more evident. Finally, considering really amorphous systems as, for instance, structurally disordered films or binary alloys, the usual techniques working very well for the crystalline phase fail completely. Aiming at a physical understanding of those systems one has to develop new mathematical approaches, and perhaps even new theoretical conceptions.

Basing on a technological interest caused by the discovery of the electrical switching behaviour of some chalcogenide glasses [1] there were many attempts to get an insight into the behaviour of the electrons moving in the potential of an amorphous semiconductor. It was N. Mott together with many others, who introduced and elaborated the concept of *localized* and *extended* electron states in order to explain transport phenomena in amorphous solids. There have been a lot of very extended studies and comprehensive reviews concerning this field [2 to 6]. The most complete is perhaps in the book by N. Mott and E. A. Davis [7] to which we refer the reader for further information.

In spite of many earlier efforts [8 to 15] it was only in 1967 when a quantitative mathematical method of calculating the electronic properties of a real nonideal solid was presented. P. Soven introduced the CPA-method for the calculation of the density of *compositionally* disordered systems [16] by introducing self consistently a complex, coherent potential simulating the scattering properties of an atom in an alloy. In the following years, the CPA-method was extended and many relatively simple models were treated in order to get an insight into the nature of the approximation and the qualitative features of the electronic spectrum [17 to 27]. The CPA-method is essentially a single – site approximation. Therefore, it cannot describe very well the electronic properties of short range ordered media as we are faced with in the cases of amorphous solids. Hence, we do not want to go into the details of this theory in the following chapters.

In the last two years, two approaches have been developed allowing the investigation of the electronic features of *structurally* disordered solids. The one starts from a tight binding ansatz and can be used to discuss the gross features of the spectrum using a model Hamiltonian [28 to 32]. The second is based on a nearly free electron model and allows us to investigate quantitatively the effect of disorder on electronic properties, i.e. the density of states and the dielectric constant [33 to 38]. Simultaneously, the experimental information concerning the electronic spectrum increased. There is a great number of new results from improved and extended optical measurements [39 to 43] dealing with the overall features of the electronic spectrum. Moreover, there are also most recent photoemission data yielding informations about fine structures in the density of states [44 to 51]. So, for the first time, we are now in the happy situation of being able to report calculations of the density of states and the imaginary part of the dielectric constant of *real* amorphous systems together with experimental data.

I. The problem

A classical experimental method of investigating the electronic spectrum of solids is the measurement of optical absorption. Photons of the energy $\hbar\omega$ are annihilated

by exciting electrons from initial states ψ_i with energies E_i to final states ψ_f with energies E_f. The imaginary part of the dielectric constant is related to the absorption coefficient of electromagnetic radiation and can be written in linear approximation as

$$\epsilon_2(\omega) \sim \frac{1}{\omega^2} \sum_{i,f} M_{if}\,\delta(E_f - E_i - \omega) \qquad (T = 0) \tag{1}$$

$M_{if} = |\langle \psi_i | \vec{e} \cdot \vec{p} | \psi_f \rangle|^2$ are the transition probabilities of the electrons. $\delta(E_f - E_i - \omega)$ represents the energy conservation law. E_i and E_f and also M_{if} depend on the structure of the solid. Hence, one expects changes in the optical absorption spectrum if one changes the atomic configuration. As an illustrative example take the ϵ_2-spectrum of crystalline (cubic) and amorphous Germanium (Fig. 1) [52, 53]. The differences between the two curves are considerable. The crystalline spectrum exhibits peaks and structures. The amorphous spectrum consists only of one broad peak. The center of mass of it is shifted to lower energies, as compared to the crystalline case. Remarkably, the spectrum of the amorphous film shows an energy gap as well as the crystalline spectrum. One obtains similar results from other materials [54].

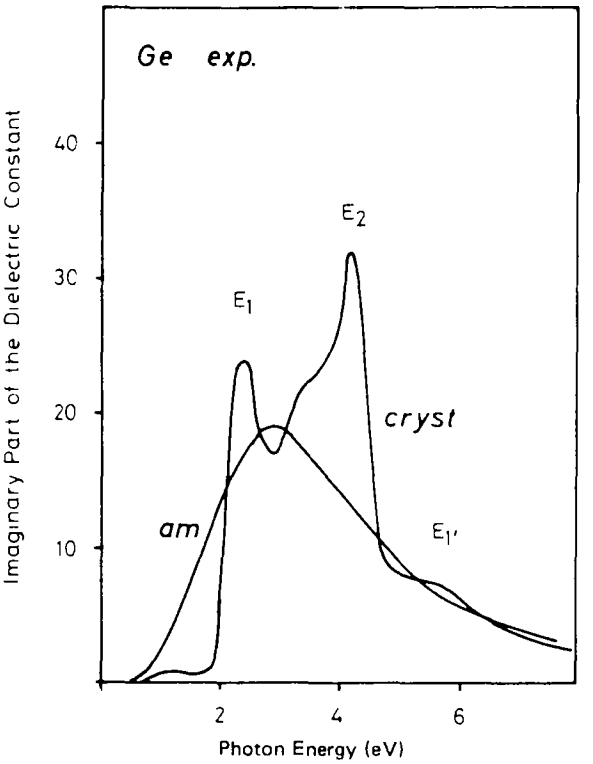

Fig. 1
The experimental ϵ_2-spectra of crystalline [52] and amorphous [53] germanium. The peaks E_1 and $E_{1'}$ of the crystalline spectrum originate in transitions near the Γ-L-axis of the Brillouin zone (see Fig. 20). E_2 belongs to transitions near X.

Since optical constants only contain energy differences, simple optical absorption measurements do not yield the complete information about the electronic energy spectrum. This difficulty can be overcome with the help of photoemission experiments. There, the final energy E_f is fixed. A photon of energy $\hbar\omega$ enters the solid, excites an electron from E_i to E_f and, if E_f is large enough, the electron can be emitted out of the bulk with a certain escape probability $P(E_f, \omega)$. The energy distribution curve, EDC (E, ω), of the photoemitted electrons is given by

$$\mathrm{EDC}(E, \omega) \sim \sum_{if} M_{if}\, \delta(E - E_i - \omega)\, \delta(E - E_f)\, P(E, \omega)\,. \tag{2}$$

Under certain conditions, it can be related to initial and final density of states features [55, 56]. As an example, Fig. 2 shows EDC – curves of a Ge – film that is

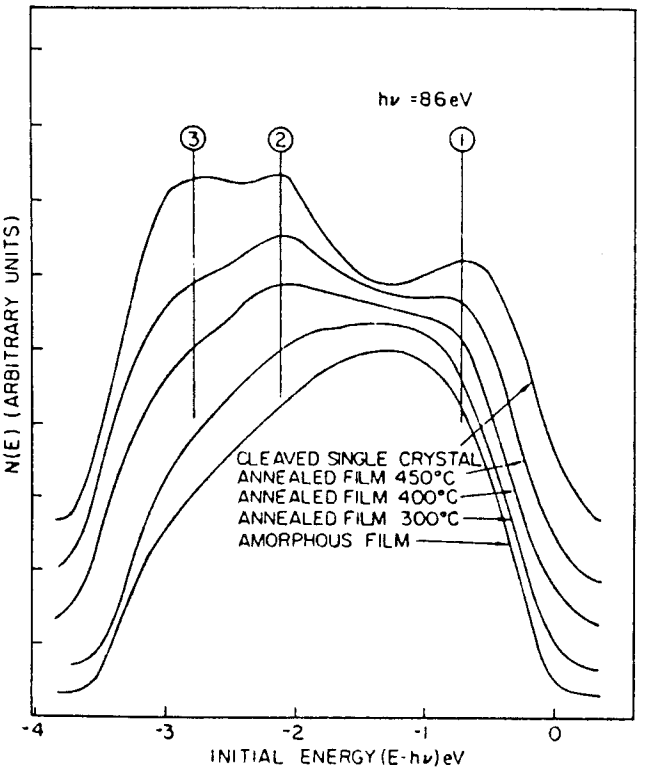

Fig. 2. Energy distribution curves of photoemitted electrons of germanium [50] The photon energy is 8.6 eV. The four curves are taken from samples annealed to transform into the crystalline phase. The uppermost curve is from a single crystal. Three pieces of structure (labelled (1) to (3)) due to direct transitions gradually appear as the material crystallizes.

transformed from the amorphous into the crystalline phase by annealing at different temperatures [50]. Again, we have a lot of structures in the crystalline case. Tracing the energy distribution curve with annealing temperature, one notices a conservation of the peak denoted by (1), whereas the structures (2), (3) are smoothed out by disorder. Obviously, different parts of the electronic energy spectrum react differently on structural disorder [54].

So far, we did not say anything about energy levels within the gap, which might occur in disordered systems. One possible way to get information about gap states is to extend optical measurements to energies below the absorption edge. This has been done by Tauc and Menth for chalkogenide glasses [57, 58]. Other possibilities are measurements of the magnetic susceptibility [57, 58] and electron spin resonance (ESR) [59]. Very exciting results are obtained by measurements of the electrical conductivity using field effect techniques [60]. These experiments yield detailed information about the density of states in the gap. An example is shown in Fig. 3. One may conclude, that the density of states in the gap is about $10^{17}-10^{18}$ and depends

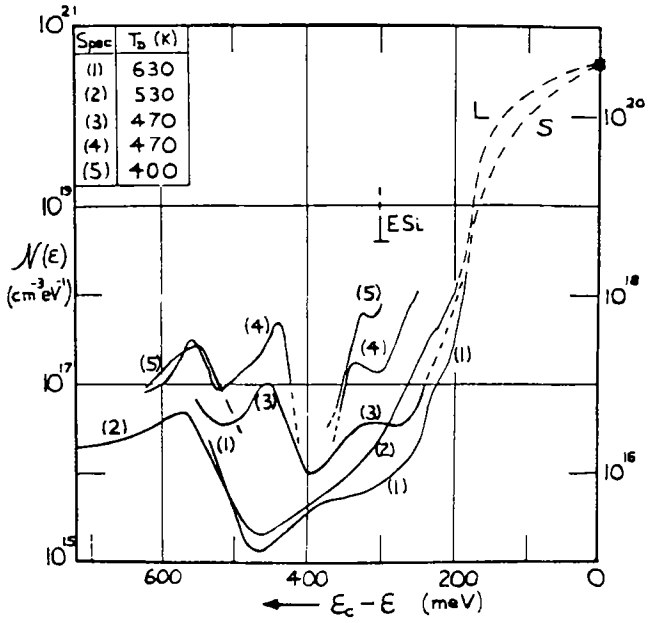

Fig. 3. The density of localized states in silicon, $N(\epsilon)$, plotted against the energy $\epsilon_c - \epsilon$. T_D is the temperature of the substrate holder during deposition. Point ESi refers to an evaporated Si specimen. L and S denote linear and square law interpolations respectively. [60].

strongly on the preparation conditions. Consequently, the states well within the energy gap are not simply caused by the lack of long range order, but are likely to be associated with defects including "dangling bonds". As has been mentioned, the problems connected with these gap states are reviewed in ref. [7]. Therefore, we shall confine ourselves to a theoretical explanation of those features of the electronic spectrum of solids, that are more clearly related to long range order and short range order, respectively, as, e.g., the selective descrease of peaks in the absorption spectrum paralleling the transition from order to disorder.

It is relatively easy to solve the problem of calculating the electronic spectrum of a crystalline system, where the long range order is defined through the points of a Bravais lattice. With the usual periodic boundary conditions the Hamiltonian of the system becomes invariant under lattice translations. Bloch's theorem can be applied. The Hamiltonian can be diagonalized with respect to the electron wave vector $\vec{k}$. The result is the well known energy band model containing the energy eigenvalues $E_m(\vec{k})$ and the respective Bloch states $\psi_{m\vec{k}}$. These can be used to calculate the electronic properties, as for example the density of states and the dielectric constant. The fundamental importance of the band structure concept must be seen in the possibility of evaluating the predominant features of the electronic properties, as, e.g., positions and shapes of peaks in the density of states and the absorption spectrum, simply by investigating the behaviour of the function $E_m(\vec{k})$.

If the atoms are distributed arbitrarily, the band model breaks down and we are right back at the beginning of the problem. It is not even possible to classify the approximately 10^{23} energy eigenvalues of the Hamiltonian. Since the number of atoms is very large, one cannot know their exact positions. It is obvious, that one cannot solve the problem in general for really arbitrary atomic configurations. One can, however, try approximative solutions by constructing structural models that take into account the chemical properties of the atoms, and experimental data concerning the atomic structure of amorphous solids. The desirable aim of the considerations should be the evaluation of an elegant and simple method to calculate electronic properties of amorphous solids, that is of comparable general bearing as the energy band structure concept for crystalline solids. In other words, we want to investigate the question of how to generalize the "band model" to solids without long range order.

II. The atomic structure of amorphous solids

The construction of a structural model is complicated by two severe constraints. On the one hand the model should be simple enough to be mathematically tractable. On the order hand it must be close enough to reality in order to allow for a reasonable quantitative interpretation of experimental results. Starting point for any struc-

tural model should be the chemical nature of the constituent atoms, which determines the types of bonds between nearest neighbors. The deviations of the directions and lengths of these bonds from given values are very small for covalently bonded semiconductors, on which we will concentrate in the following. For details of the chemistry of amorphous solids the reader is referred to ref. [61]. The main point we want to stress here is the necessity to take into account the short range order to get a realistic model of an amorphous semiconductor.

As has been mentioned already, the most simple possibility of constructing a solid is to assume identical atoms to be situated at the points of a crystal lattice (Fig. 4a). In this case the bond directions and lenghts have fixed values. The crystalline structure exhibits long range order as well as short range order. It can be defined by a set of lattice vectors $\vec{R}_l$ denoting the core sites. Starting from a crystalline structure one obtains more complicated systems in two ways: The first is to replace statistically some of the, say A-atoms of the crystal by B-atoms. One may call this a compositionally disordered structure (Fig. 4b). If the concentration of the B-atoms is small compared with that of the A-atoms, the problem is essentially the calculation of the spectrum of an impurity in a crystal. If the concentration of the B-atoms is comparable to that of the A-atoms we are left with the calculation of the electronic-spectrum of an alloy. The second way of introducing disorder is to allow the bond-

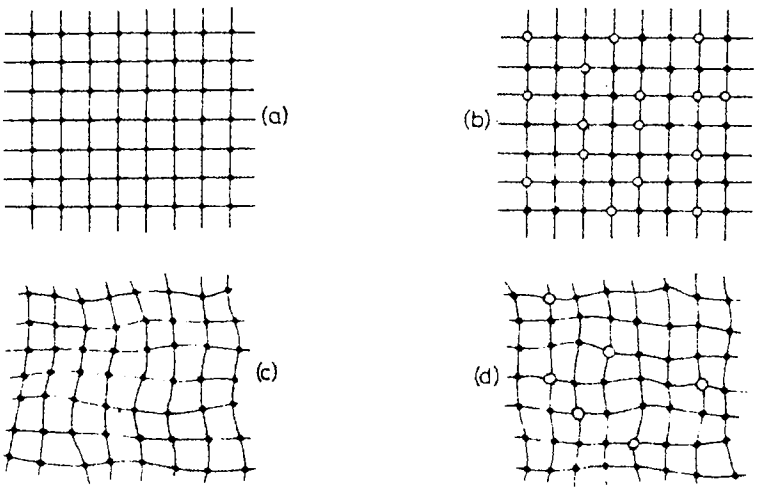

Fig. 4. Two-dimensional models for amorphous solids.

a) crystalline structure with perfect short range order and long range order.
b) compositionally disordered system consisting of two types of atoms distributed randomly at the sites of a crystal lattice.
c) structurally disordered system with short range order but no long range order.
d) mixed system exhibiting structural and compositional disorder.

ing lengths and angles to vary a little bit about the crystalline values. The result is a structurally disordered system containing still short range order, but no long range order (Fig. 4c). In principle it is possible to describe this structure by the crystalline values of bond lengths and angles and by the amount of the deviations from these values weighted with a certain probability function. Obviously, one may construct still other more complicated amorphous models, for example, by mixing compositional and structural disorder (Fig. 4d).

The proceed with the discussion it is very instructive to look at structural measurements. Fig.'s 5 and 6 show Laue patterns of Se-films deposited at different temperatures [62]. The intensity distribution of Laue diagrams is essentially given by the Fourier transformed spatial distribution of atoms in the solid [63]. In a crystalline phase, the atom distribution can be described by a sum of delta functions

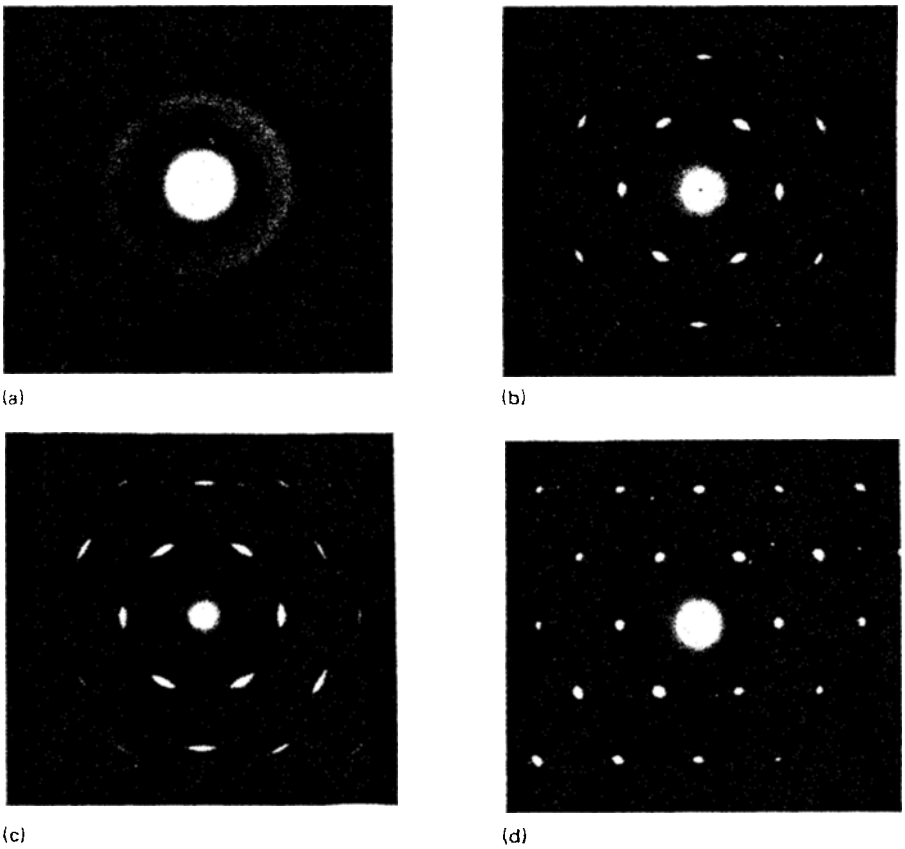

Fig. 5. Lauc patterns of selenium films on (0001) tellurium deposited at different substrate temperature. a) 40 °C, b) 60 °C, c) 80 °C, d) 120 °C [62].

centered at the lattice sites. The Fourier transform, $F(\vec{q})$, of such a distribution is a sum of delta functions centered at the reciprocal lattice points, which appear therefore as sharp points of high intensity in the pattern. In the more general case of a crystal with m atoms in the unit cell the intensity of the points is modulated by an amplitude factor containing the structure of the unit cell (Fig.' 5d and 6d).

$$F(\vec{q}) \sim \sum_{n} \sum_{j} e^{\vec{K}_n \vec{a}_j} \delta(\vec{q} - \vec{K}_n) . \tag{3}$$

$\vec{a}_j$ are the position vectors of the atoms in the unit cell. $\vec{K}_n$ are the reciprocal lattice vectors.

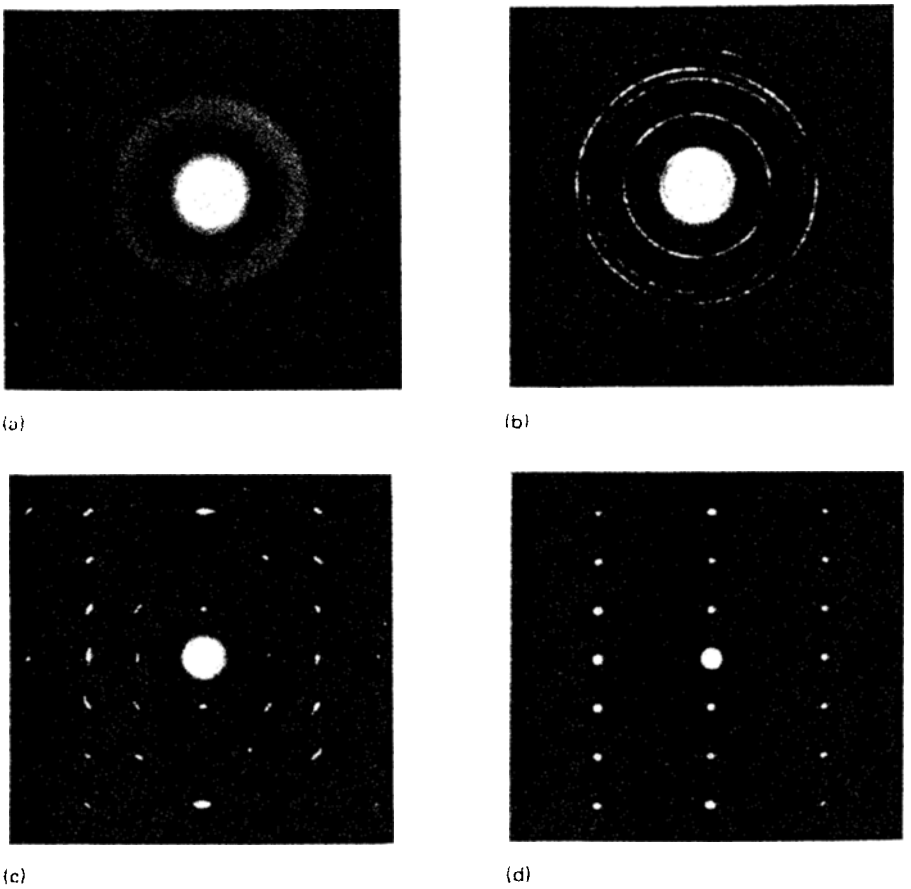

Fig. 6. Laue patterns of selenium films on $(10\bar{1}0)$ tellurium at a) 40 °C, b) 60 °C, c) 80 °C, d) 120 °C substrate temperatures [62].

If the crystalline structure is disturbed by small statistical deviations of the bond parameters from their crystalline values, the sharp dots in the Laue pattern will be broadened. Variations in bond lengths cause broadening in radial direction. Variations in bond angles give rise for a broadening in angular direction. Hence, Fig.' 5c, 5b, and 6c correspond with polycrystalline phases with rather small fluctuations in the orientations of the crystallites. Fig. 6b belongs to a polycrystalline

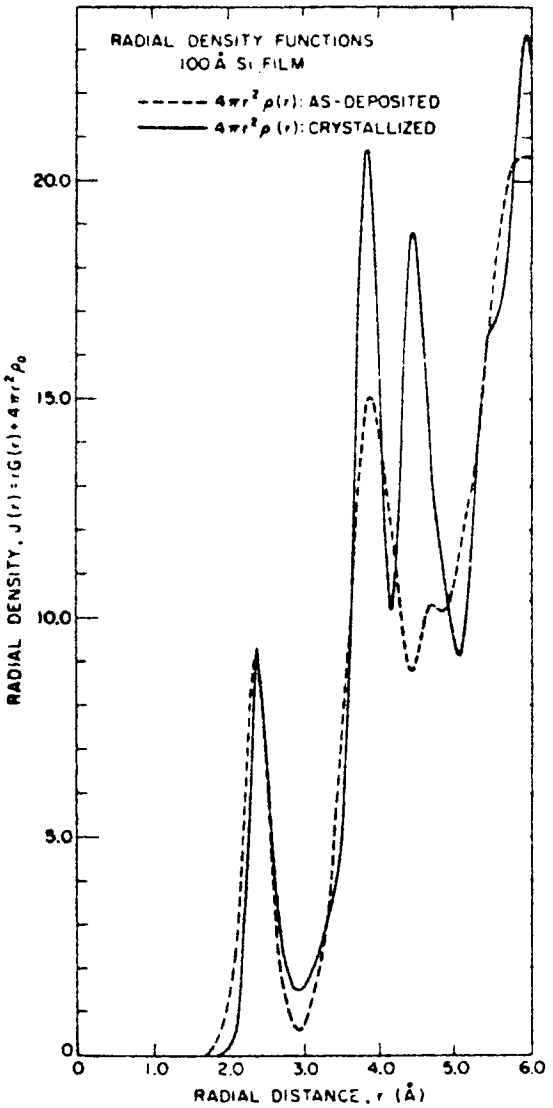

Fig. 7
Atomic distribution curves of crystalline and amorphous silicon [65]. The similarity in sharpness of the first peak demonstrates the small variation in nearest neighbor bonds in the amorphous film. The increase in beadth of the second amorphous peak is attributed to appreciate tetrahedral bond angles disortions. The vanishing of the third peak in the amorphous curve can be explained by a certain amount of eclipsed configurations of tetrahedrons occuring in the amorphous phase [69, 70] (see also Fig. 8).

phase consisting of randomly oriented trigonal crystallites and some other structure, perhaps α-monoclinic. Fig.'s 5a and 6a are taken from amorphous phases. The radius of the broad ring around the origin of the amorphous pattern is approximately the distance of the crystalline second neighbored dots from the origin in Fig. 6d. Each point of the crystalline diffraction pattern represents three atoms, because the unit cell of trigonal Se contains three atoms. Therefore, it is very difficult to draw definite conclusions on details of the short range order. Only a rough estimate of the diameter of the short range order volume is possible. For amorphous Se it should be four times the diameter of the unit cell of trigonal Se.

Informations about the coordination numbers of amorphous solids can readily be obtained from x-ray measurements of the radial atomic distribution function [64 to 68]. As an example, the atomic distribution curves of crystalline and amorphous Silicon films are plotted in Fig. 7 [65]. The interpretation of the curves shows that the mean positions and the numbers of the nearest neighbors are almost the same in the amorphous and in the crystalline phase. This holds for the second nearest neighbors, too. The peak belonging to the third neighbors vanishes in the amorphous phase. Detailed investigations have explained this feature by assuming the occurance of "staggered" and "eclipsed" configurations of tetrahedrons in the amorphous modifications of Ge and Si (Fig. 8) [69 to 71].

The conservation of the nearest neighbor coordination is valid not only in Ge and Si but also in other elemental and compound semiconductors [61, 67, 68]. Amorphous materials exhibit the same short range order as the corresponding crystalline modifications. It is this property, that forms the basis of our considerations in the following chapters.

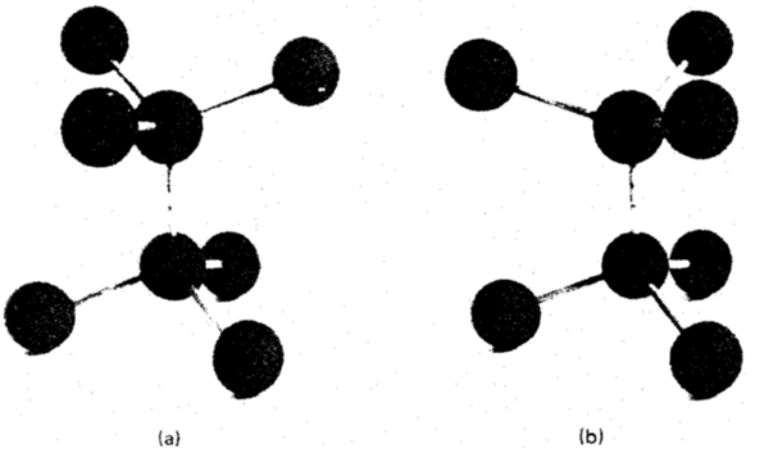

Fig. 8. Possible configurations of tetrahedrons in disordered tetrahedrally bonded systems. a) staggered configuration, b) eclipsed configuration.

III. Basic equations

III.1. The Schrödinger equation

To discuss the electronic properties of solids one can start with the Schrödinger equation in one electron approximation.

$$H^{\vec{\rho}_1 \cdots \vec{\rho}_N} \left| \psi_\lambda^{\vec{\rho}_1 \cdots \vec{\rho}_N} \right\rangle = E_\lambda^{\vec{\rho}_1 \cdots \vec{\rho}_N} \left| \psi_\lambda^{\vec{\rho}_1 \cdots \vec{\rho}_N} \right\rangle . \tag{4}$$

H is the sum of the kinetic energy of the electron and the potential of the N atom cores.

$$H^{\vec{\rho}_1 \cdots \vec{\rho}_N} = H_0 + V^{\vec{\rho}_1 \cdots \vec{\rho}_N} . \tag{5}$$

H depends on the positions, $\vec{\rho}_1 \cdots \vec{\rho}_N$, of the atoms, so do the solutions of equ. (4), the energy eigenvalues E_λ and the respective wave functions. In the case of a local electrostatic potential we have in space coordinates

$$V(\vec{r}) = \sum_{l=1}^{N} v(\vec{r} - \vec{\rho}_l) \tag{6}$$

where $v(\vec{r})$ is an atomic potential.

Using the solutions of the Schrödinger equation one can calculate the density of states.

$$n^{\vec{\rho}_1 \cdots \vec{\rho}_N}(E) = \frac{1}{N} \sum_{\lambda} \delta(E - E_\lambda^{\vec{\rho}_1 \cdots \vec{\rho}_N}) . \tag{7}$$

The imaginary part of the dielectric constant can be written as

$$\epsilon_2(\omega) \sim \frac{1}{\omega^2} \sum_{\lambda\lambda'} |\langle \psi_\lambda | \vec{e} \cdot \vec{p} | \psi_{\lambda'} \rangle|^2 \cdot \delta(E_\lambda + \omega - E_{\lambda'}) F(T; E_\lambda, E_{\lambda'}) \tag{8}$$

$\vec{e}$ is the polarization vector of the electromagnetic waves, $\vec{p}$ the momentum operator, ω the photon energy, and $F(T; E_\lambda, E_{\lambda'})$ the temperature dependent probability of finding an occupied initial state E_λ and a nonoccupied final state $E_{\lambda'}$.

For arbitrary configurations without any symmetry properties it is impossible to evaluate the solutions of equ. (4). Therefore, we shall outline in the following section a method that takes into account a little more the statistical nature of the problem.

III.2. The resolvent method

The density of states and the imaginary part of the dielectric constant of a macroscopic system can be written as

$$n(E) = -\frac{1}{\pi} \operatorname{Tr} \operatorname{Jm} G(E^+) \tag{9}$$

$$\epsilon_2(\omega) \sim \frac{1}{\omega^2} \int dE \operatorname{Tr} [(\vec{e} \cdot \vec{p}) \operatorname{Jm} G(E^+ + \omega) \times (\vec{e} \cdot \vec{p}) \operatorname{Jm} G(E^+)] F(T; E, \omega) \tag{10}$$

$\epsilon_2(\omega)$ contains no electron hole interaction. $\vec{e}$, $\vec{p}$, $F(T; E, \omega)$ are defined quite analoguously as before. The one electron propagator, $G(E^+)$, is given by

$$G^{\vec{\rho}_1 \cdots \vec{\rho}_N}(E^+) = \frac{1}{E^+ - H^{\vec{\rho}_1 \cdots \vec{\rho}_N}} \tag{11}$$

E^+ means, that the energy parameter includes a small, nonzero positive imaginary part in order to avoid singularities on the real energy axis. This small imaginary part has to be taken equal to zero after finishing the calculation. H is the structure dependent Hamiltonian of the system. Using the eigenvalues and eigenfunctions of H one finds the spectral representation of $G(E^+)$.

$$G(E^+) = \sum_\lambda \frac{|\psi_\lambda\rangle\langle\psi_\lambda|}{E^+ - E_\lambda} \tag{12}$$

and equ's (9) and (10) reduce to the usual expressions.

From equ's (9) and (10) it is obvious that instead of solving the Schrödinger equation one can calculate the resolvent $G(E^+)$. The poles of G in the complex energy plane are the eigenvalues of H and the residues of G contain the respective wave functions. G depends on the configuration of atoms, so do $n(E)$ and $\epsilon_2(\omega)$. The details of the atomic configuration are unknown. Therefore, one has to take the configurational averages of equ's (9) and (10). That means in the case of $n(E)$ the averaging of the one electron propagator

$$g^{(1)}(E^+) := \int \cdots \int d^3\vec{\rho}_1 \ldots d^3\vec{\rho}_N \, P(\vec{\rho}_1 \ldots \vec{\rho}_N) \, G^{\vec{\rho}_1 \cdots \vec{\rho}_N}(E^+) . \tag{13}$$

In the case of ϵ_2 one has to average the product of two one electron propagators.

$$g^{(2)}(E^+, \omega) := \int \cdots \int d^3\vec{\rho}_1 \ldots d^3\vec{\rho}_N \, P(\vec{\rho}_1 \ldots \vec{\rho}_N) \times G^{\vec{\rho}_1 \cdots \vec{\rho}_N}(E^+ + \omega) (\vec{e} \cdot \vec{p}) \, G^{\vec{\rho}_1 \cdots \vec{\rho}_N}(E^+) \tag{14}$$

$P(\vec{\rho}_1 \ldots \vec{\rho}_N)$ is the normalized probability of finding a configuration $\vec{\rho}_1 \ldots \vec{\rho}_N$.

Using equ. (5) one can elaborate an integral equation for G by expanding the expression (11).

$$G(E^+) = G_0(E^+) + G_0(E^+)VG(E^+). \tag{15}$$

$G_0(E^+) = (E^+ - H_0)^{-1}$ is the free electron propagator. Iterating equ. (15) we get the Born series for G.

$$G = G_0 + G_0 V G_0 + G_0 V G_0 V G_0 + G_0 V G_0 V G_0 V G_0 + \ldots . \tag{16}$$

If V is a weak potential one can neglect the higher order terms in equ. (16). The result is the Born approximation well known from first order scattering theory. Unfortunately, in the case of a solid V is not a weak potential and we are left with the problem of summing the whole infinite series.

IV. Simple models

IV.1. A tight binding model

In principle, one might assume the tight binding approximation to be suitable for the problem because the atomic positions occur explicitly in the Hamiltonian. Further inspection of the equ. (4), however, shows, that one needs to diagonalize a secular determinant the dimension of which is of the order of N [72 to 74]. Nevertheless, one can get from it first informations about the energy spectrum and we shall stress this point in the next few sections following the arguments of Weaire and Thorpe [28 to 32].

It is convenient to rewrite the Hamiltonian (5) into a form more suitable for a tight binding formalism by using a set of orthonormal basis functions ϕ_{lj} associated with the atomic positions $\vec{\rho}_l$ and the bonds j.

$$H = \sum_{ll'} \sum_{jj'} H_{ll'}^{jj'} \left| \phi_{lj} \right\rangle \left\langle \phi_{l'j'} \right| \tag{17}$$

$H_{ll'}^{jj'}$ are the matrix elements of H in ϕ_{lj}-representation. In the following the matrix elements are assumed to be nonzero only between basis functions associated with the same atom or the same bond. For a fixed atom and different bonds, they are equal to V_1, for a fixed bond and different atoms equal to V_2. Only nearest neighbors are taken into account. The resulting model Hamiltonian is

$$\hat{H} = V_1 \sum_{l} \sum_{j \neq j'} \left| \phi_{lj} \right\rangle \left\langle \phi_{lj'} \right| + V_2 \sum_{l \neq l'} \sum_{j} \left| \phi_{lj} \right\rangle \left\langle \phi_{l'j} \right| . \tag{18}$$

In the special case of a tetrahedrally coordinated structure, to which we shall restrict the discussion of this chapter, the number of nearest neighbors and, hence, the number of bonds is four. For $V_2 = 0$ the Hamiltonian (18) describes completely decoupled atoms with a singly degenerate (s-like) eigenstate at $E = 3\ V_1$ and a triplet at $E = -V_1$. For $V_1 = 0$ we have decoupled bonds associated with doublets at $E = \pm V_2$ being of bonding and antibonding character.

In order to derive the general properties of the electronic spectrum one has to make the additional assumption of bounded variation of density. This means, that a volume can be defined, so that the number of atoms in this volume is bounded above and below, the lower limit being nonzero.

Writing the solution ψ of the Schrödinger equation

$$\hat{H}\,\psi = E\,\psi \tag{19}$$

as a superposition of the basis functions ϕ_{lj} with coefficients a_{lj} one obtains a matrix equation

$$M\,\vec{u}\,(l) = -V_2\,\vec{v}\,(l) \tag{20}$$

where $\vec{u}\,(l)$ and $\vec{v}(l)$ are four-component vectors defined by

$$\begin{aligned} \vec{u}(l) &= \{\, a_{l1} \ldots a_{l4} \,\} \\ \vec{v}(l) &= \sum_{l \neq l'} \{\, a_{l'1} \ldots a_{l'4} \,\} \end{aligned} \tag{21}$$

M is the matrix

$$M = \begin{pmatrix} -E & V_1 & V_1 & V_1 \\ V_1 & -E & V_1 & V_1 \\ V_1 & V_1 & -E & V_1 \\ V_1 & V_1 & V_1 & -E \end{pmatrix} \tag{22}$$

M has eigenvalues

$$\begin{aligned} \lambda_s &= -E + 3\,V_1 \qquad \text{(singly degenerate)} \\ \lambda_p &= -E - V_1 \qquad \text{(triply degenerate)} \end{aligned} \tag{23}$$

Discussion of the properties of the solutions of equ. (20) yields energy regions, where the density of states vanishes in the limit $N, \Omega \to \infty$ if the following conditions hold:

$$\begin{aligned} &\max.\ (\lambda_n^2) < V_2^2 \\ &\min.\ (\lambda_n^2) > V_2^2 \end{aligned} \qquad n = s, p \tag{24}$$

From these relations one obtains the magnitude of the energy gap to be

$$E_G = 2|V_2| - 4|V_1| \qquad (V_1/V_2 < 1/2) \tag{25}$$

Superposing the solutions of equ. (20) by the s-like and p-like eigenvectors of M

$$\vec{u} = c_s \vec{u}_s + c_p \vec{u}_p \tag{26}$$

one can discuss the nature of the wave functions belonging to the different energy bands by investigating their fractional s and p character

$$\begin{aligned} F_s &:= \sum_{l=1}^{N} |c_s(l)|^2 \\ F_p &:= \sum_{l=1}^{N} |c_p(l)|^2 \end{aligned} \tag{27}$$

Using the eigenvalues of M one has

$$\begin{aligned} F_s &= \frac{\lambda_p^2 - \lambda_s^2}{\lambda_p^2 - V_2^2} \\ F_s + F_p &= 1 \,. \end{aligned} \tag{28}$$

Similarly one may calculate the fractional bonding character of the wave functions.

$$F_b := \frac{1}{2}\left(1 + \sum_{l=1}^{N} \vec{u}^*(l) \cdot \vec{v}(l)\right). \tag{29}$$

Evaluation in terms of F_s and F_p yields

$$F_b = \frac{1}{2}\left(1 - \frac{\lambda_s F_s + \lambda_p F_p}{V_2}\right) \tag{30}$$

Fig.' 9 to 10 show these results graphically.

A restrictive assumption used in the analysis was that of constant overlap parameters V_1 and V_2. Nonconstant overlap integrals, for example due to deviations of the bond angles from the ideal values lead to a decrease in the gap width [30]. Particularly, if V_1 and V_2 are allowed to vary in intervals

$$V_1 = \bar{V}_1 \pm \Delta_1, \quad V_2 = \bar{V}_2 \pm \Delta_2 \tag{31}$$

one finds a gap of the magnitude

$$E_G = 2(|\bar{V}_2| - \Delta_2) - 4(|\bar{V}_1| + \Delta_1) \qquad (\bar{V}_1/\bar{V}_2 < 1/2)\,. \tag{32}$$

It is also possible to proof the existence of a band gap if the overlap between different atoms and different bonds is taken into consideration. For tetrahedrally bonded compound semiconductors one obtains similar results.

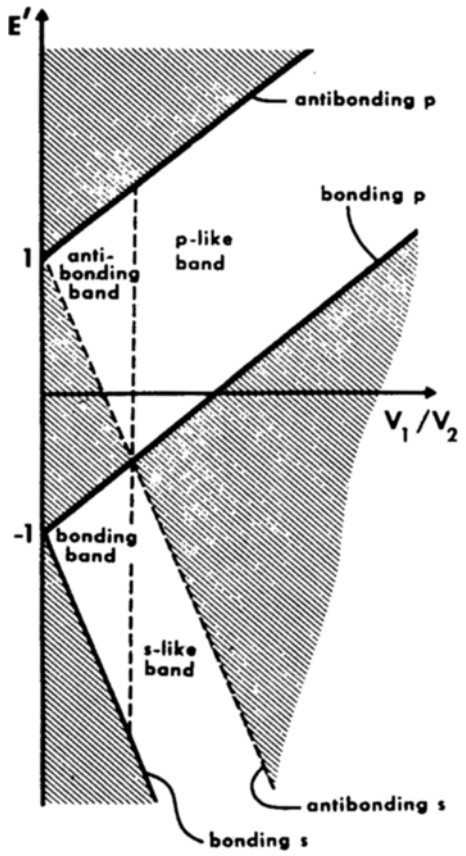

Fig. 9
Bounds on the density of states of tetrahedrally coordinated solids, and various features of the allowed bands. $E' = E/V_2$. Shaded regions are forbidden, unshaded are allowed. The heavy lines are associated with delta functions in the density of states [29].

The solution of the Schrödinger equation (19) requests still the diagonalization of a $4N \cdot 4N$ dimensional secular determinant. The dimension of the determinant can be reduced only in the case of a crystalline structure because then the ansatz functions ϕ_{Ij} can be chosen to have Bloch character. One obtains analytical expressions for the eigenvalue spectrum and the density of states. The result is plotted in Fig. 11 together with the density of states of Ge calculated by use of a more realistic model [85]. The shape of the lowest valence band is reproduced quite well by the present model calculation. The higher bands agree only qualitatively. Particulary, the uppermost valence band being rather broad in the realistic calculation is reduced to a delta peak in the model. This indicates a flat, $\vec{k}$-independent energy band in the electronic band structure. The conduction band does not show any similarity at all. This is just the statement that a tight binding approach with a finite set of ansatz functions is suitable only for valence bands – the deeper, the better. Nevertheless, one can assume that at least qualitative features of the density of states are described sufficiently well.

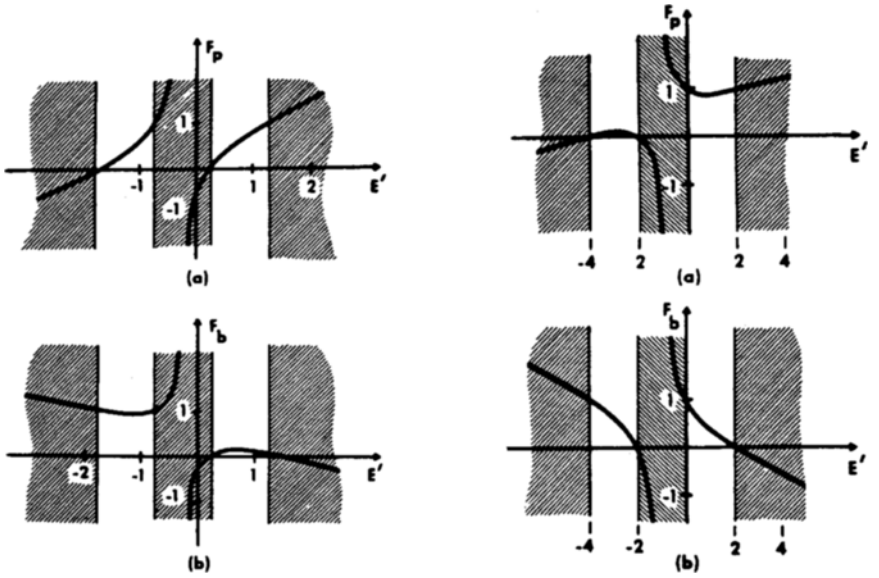

Fig. 10. Left hand side: Fractional p-like character, F_p, and bonding character, F_b, of wave functions. $V_2 = -1$, $V_1 = -1/4$. Right hand side: F_p and F_b for $V_2 = -1$ and $V_1 = -1$ [29]

In order to get an insight into the behaviour of the bands with disorder, Weaire and Thorpe considered the Bethe lattice (Fig. 12) [30], a mathematical artifact allowing to evaluate the density of states of a macroscopical system analytically without referring to structural properties except the next neighbors coordination. The density of states of the Bethe lattice calculated using the same parameters as in the crystalline case is rather featureless except the delta function representing the uppermost valence band (Fig. 11).

IV.2. The nondirect transition method for the calculation of optical absorption spectra

To derive optical properties one can use a qualitative argument obtained by comparing the gross structures of an amorphous and a crystalline phase. The essential feature of a crystalline phase is the long range order giving rise for the $\vec{k}$-selection rule in optical transitions.

$$\epsilon_2(\omega) \sim \frac{1}{\omega^2} \int_{-\omega}^{0} dE \int d^3\vec{k} \int d^3\vec{k}' \sum_{m\,m'} |\langle \psi_{m\vec{k}} | \vec{e}\,\vec{p} | \psi_{m'\vec{k}'} \rangle|^2 \times$$
$$\times\, \delta(E - E_m(\vec{k}))\, \delta(E + \omega - E_{m'}(\vec{k}')) \tag{33}$$

$\psi_{m\vec{k}}$ and $\psi_{m'\vec{k}'}$ are the Bloch functions belonging to the energy bands $E_m(\vec{k})$ and $E_{m'}(\vec{k}')$.

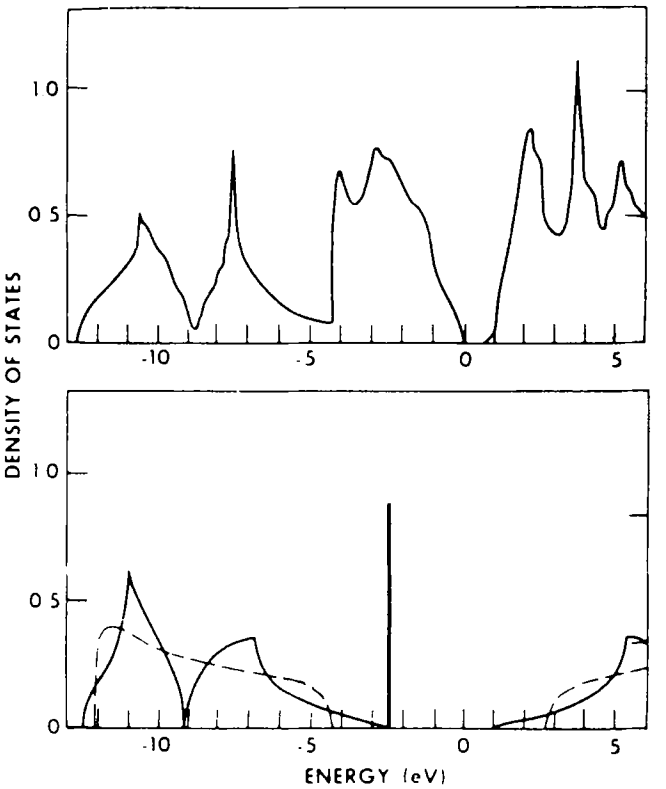

Fig. 11. Density of states of germanium [32]. Top: as calculated by Herman et al. [85]. Bottom: calculated using the tight binding model with $V_1 = -2.5$ eV, $V_2 = -6.75$ eV. The solid line refers to the crystal, the dashed line to the Bethe lattice (Fig. 12). The delta function indicated by a vertical line is found in both structures. Units are states/(eV atom)

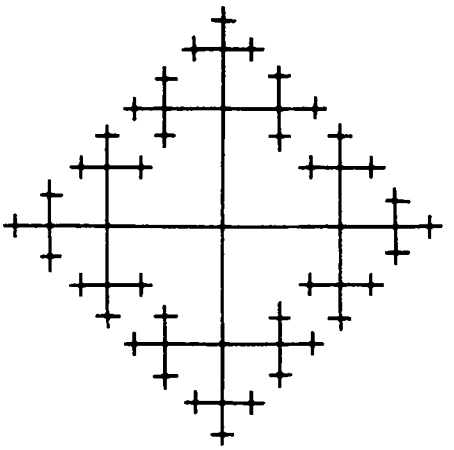

Fig. 12. The Bethe lattice [30]. The lines represent the bonds connecting each atom to its neighbors.

A disordered structure does not show any long range order. Consequently, k is not a good quantum number. Hence, there is no $\vec{k}$-selection rule and the $\vec{k}$-integration in equ. (33) can be evaluated separately. This yields the well known nondirect transition equation for the optical absorption [75 to 78].

$$\epsilon_2(\omega) \sim \frac{1}{\omega^2}\,\overline{M(\omega)} \int_{-\omega}^{0} dE\, n_v(E)\, n_c\,(E+\omega)\,. \tag{34}$$

$\overline{M(\omega)}$ is the averaged transition probability. n_v and n_c are the density of states of the valence band and the conduction band, respectively. If n_v and n_c are assumed to be approximately the same as in the crystal, all information about the disorder are involved in $\overline{M(\omega)}$. In the crystalline phase $\overline{M(\omega)}$ shows pronounced peaks besides a decrease with photon energy (Fig. 13). In the amorphous phase one expects these *umklapp-enhanced* peaks to be completely smeared out leaving behind a smooth, monotonically decreasing function. As an example, the ϵ_2-spectra of amorphous Ge and Si calculated by using equ. (34) are plotted in Fig. 14.

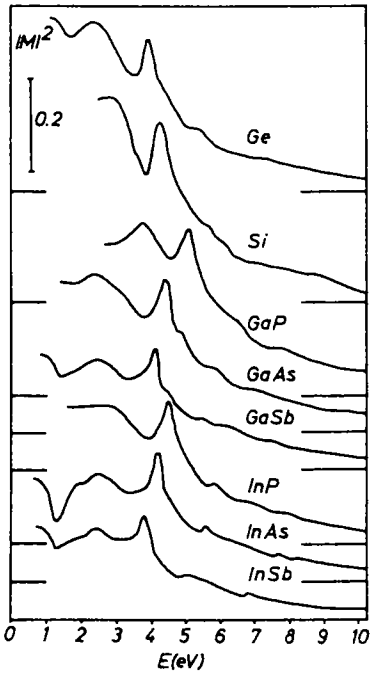

Fig. 13
Average crystalline transition probabilities of the tetrahedrally bonded semiconductors. The sharp peak occuring at about 4 eV is due to umklapp-enhancement [38].

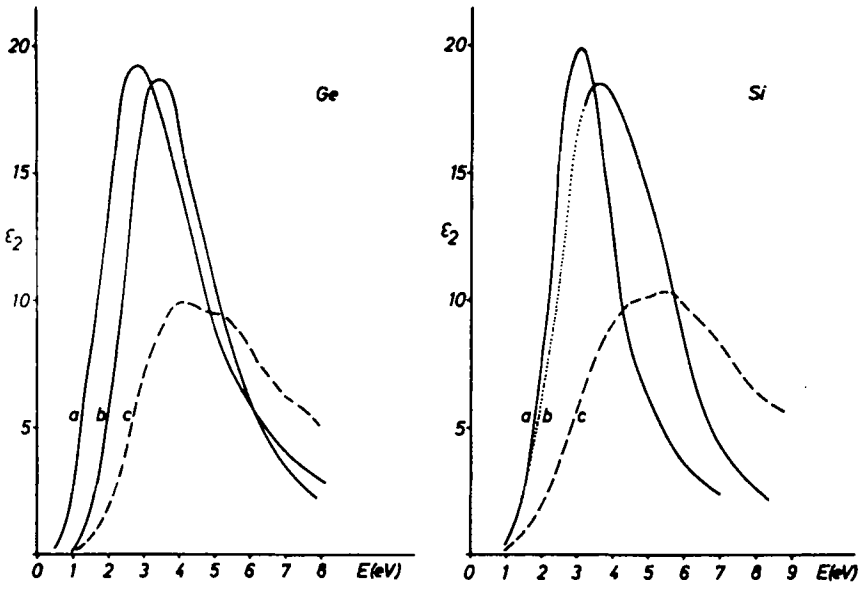

Fig. 14. The imaginary part of the dielectric constant, $\epsilon_2(\omega)$, of amorphous germanium and silicon. a) experimental curves, b) as calculated by using the nondirect transition model with energy dependend transition probabilities, c) with constant transition probabilities [38].

Unfortunately, there is no explicit connection between the structure of the solid and the optical spectrum. To discuss the disorder behaviour of the different parts of the ϵ_2-spectrum, one could refine the nondirect transition method by considering indirect transitions only in certain subregions of the $\vec{k}$-space. The difficulty remains, however, how to choose those regions. Moreover, there is no simple possibility of calculating the averaged transition probabilities the knowledge of which is essential.

V. The pseudopotential approach

The tight binding approach is suitable for the lower energy bands. In its simplest form it yields only a general view of the electronic spectrum. Therefore, it is resonable to look for a method more suitable for practical applications. To this end, we shall calculate now the density of states and the imaginary part of the dielectric constant by use of the resolvent method. In doing so, we shall start just from the opposite aspect of the problem of the electronic structure of solids: the nearly free electron approximation.

V.1. Configurational averaging

Introducing $\vec{k}$-representation and using equ. (6) one can evaluate equ. (16) in powers of $(G_0 v)$ multiplied by phase factors containing the atomic positions. Taking the configurational average one obtains the averaged Green's function.

$$
\begin{aligned}
g(\vec{k},\vec{k}';E^+) = {} & G_0(\vec{k};E^+)\,\delta(\vec{k}-\vec{k}') \\
& + \int_{\vec{\rho}_1} D_1(\vec{\rho}_1)\, e^{i\vec{k}\vec{\rho}_1}\, G_0(\vec{k};E^+)\, v_{\vec{k}\vec{k}'}\, G_0(\vec{k}';E^+)\, e^{-i\vec{k}'\vec{\rho}_1} \\
& + \int_{\vec{\rho}_1}\int_{\vec{\rho}_2} D_2(\vec{\rho}_1,\vec{\rho}_2) \sum_{\vec{k}_1} e^{i\vec{k}\vec{\rho}_1}\, G_0(\vec{k};E^+)\, v_{\vec{k}\vec{k}_1}\, e^{-i\vec{k}_1(\vec{\rho}_1-\vec{\rho}_2)} \times \\
& \quad \times G_0(\vec{k}_1;E^+)\, v_{\vec{k}_1\vec{k}'}\, G_0(\vec{k}';E^+)\, e^{-i\vec{k}'\vec{\rho}_2} \qquad (35) \\
& + \int_{\vec{\rho}_1}\cdots\int_{\vec{\rho}_3} D_3(\vec{\rho}_1 \ldots \vec{\rho}_3) \sum_{\vec{k}_1}\sum_{\vec{k}_2} e^{i\vec{k}\vec{\rho}_1}\, G_0(\vec{k};E^+)\, v_{\vec{k}\vec{k}_1}\, e^{-i\vec{k}_1(\vec{\rho}_1-\vec{\rho}_2)} \times \\
& \quad \times G_0(\vec{k}_1;E^+)\, v_{\vec{k}_1\vec{k}_2}\, e^{-i\vec{k}_2(\vec{\rho}_2-\vec{\rho}_3)}\, G_0(\vec{k}_2;E^+)\, v_{\vec{k}_2\vec{k}'} \times \\
& \quad \times G_0(\vec{k}';E^+)\, e^{-i\vec{k}'\vec{\rho}_3} \\
& + \ldots
\end{aligned}
$$

with

$$G_0(\vec{k};E^+) = (E^+ - k^2)^{-1}$$

and

$$v_{\vec{k}\vec{k}'} = \frac{N}{\Omega}\int d^3\vec{r}\, v(\vec{r})\, e^{-i(\vec{k}-\vec{k}')\vec{r}} \,.$$

The function $D_n(\vec{\rho}_1 \ldots \vec{\rho}_n)$ correlates the scattering behaviour of n atoms at the sites $\vec{\rho}_1 \ldots \vec{\rho}_n$. The sums over the atomic sites and the integrations over the N−n free variables in $P(\vec{\rho}_1 \ldots \vec{\rho}_N)$ are included in D_n. D_n contains delta functions representing multiple scattering terms [12, 13].

Generally, the calculation of the averaged Green's function is a very complicated procedure because one has to treat separately multiple scattering terms, i.e.terms, where some of the atomic positions are equal [8 to 13]. This requests partial summation techniques, and renormalization of the atomic potential. In order to get information about the electronic properties of short range ordered media one has to take into account also correlations between more than two atoms.

It is impossible to treat correctly multiple scattering at several atoms (molecule scattering), and atomic correlations of higher order than two. So, one cannot describe correctly the electronic properties of a short range ordered structure. Already in the simple case of a uniform atomic distribution as in a liquid system the partial summation procedure results in a highly nonlinear integral equation for the averaged Green's function. It can be solved only in some special cases [8 to 15, 79]. Hence, it seems reasonable to try an approximative solution by starting from the crystal that allows an exact mathematical treatment of the Born series.

The essential assumption one has to make is the following. In analogy to the crystalline case the n-atom correlation function is factorized into a product of two-atom correlation functions.

$$D_n(\vec{\rho}_1 \ldots \vec{\rho}_n) = D_2(\vec{\rho}_1 \vec{\rho}_2)\, D_2(\vec{\rho}_2 \vec{\rho}_3) \ldots D_2(\vec{\rho}_{n-1} \vec{\rho}_n) \quad . \tag{36}$$

Each two-atom correlation function can be written as a sum of functions localized at the points $\vec{R}_l$ of a suitable crystal lattice guaranteeing the presence of a short range order (Fig. 15).

$$D_2(\vec{\rho}, \vec{\rho}') = \sum_{l=1}^{N} P_l(\vec{\rho} - \vec{\rho}' - \vec{R}_l) \, . \tag{37}$$

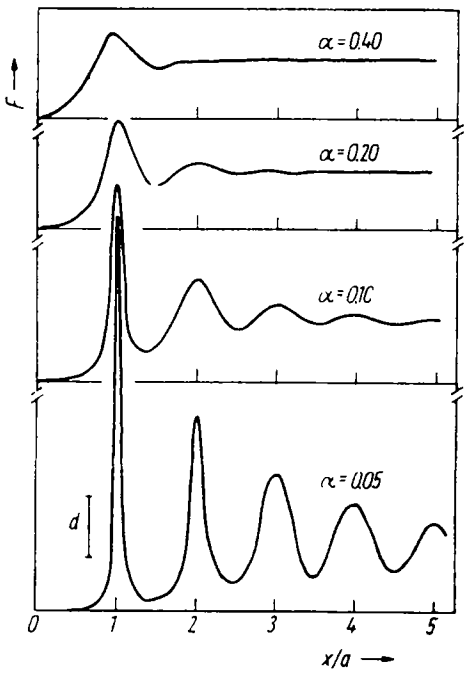

Fig. 15
Qualitative picture of the two atom correlation function $F(x) = \sum_n f_n(x; R_n)$ (one-dimensional model). The single contributions $f_n(x; R_n)$ are Gaussians localized near the lattice points $n \cdot a$, $n = 1, 2, 3 \ldots$ (a = lattice constant). The width is $\alpha \cdot n \cdot a$. For small α there are well localized maxima at the lattice points. With increasing α the number of these peaks decreases indicating a decrease of the volume of short range order [33].

The form of the single contributions have to be chosen such that

$$\lim_{\vec{\rho} \to \vec{\rho}'} D_2(\vec{\rho}, \vec{\rho}') = \delta(\vec{\rho} - \vec{\rho}')$$

$$\lim_{|\vec{\rho} - \vec{\rho}'| \to \infty} D_2(\vec{\rho}, \vec{\rho}') = \text{const} \tag{38}$$

$$\lim_{\text{width of localization} \to 0} D_2(\vec{\rho}, \vec{\rho}') = \sum_l \delta(\vec{\rho} - \vec{\rho}' - \vec{R}_l) .$$

This form of the correlation functions gives the possibility of carrying out the $\vec{\rho}$-integrations successively. The Fourier transformed two-atom correlation function is a sum of functions localized at the reciprocal lattice points, $\vec{K}_n$, with a certain width, say $\lambda(\vec{K}_n)$.

$$h_2(\vec{k} - \vec{q}) \sim \sum_n f_n(\vec{k} - \vec{q} - \vec{K}_n) . \tag{39}$$

Principally, $D_2(\vec{\rho}, \vec{\rho}')$ and hence, $h_2(\vec{k} - \vec{q})$ can be determined from structural measurements. For $\lambda \to 0$ we have $f_n \to \delta(\vec{k} - \vec{q} - \vec{K}_n)$, the Fourier transformed two-atom distribution function of a crystal.

A second assumption needed to perform the $\vec{k}$-integrations in equ. (35) is that the atomic potential $v(\vec{k} - \vec{k}') =: v(\vec{q})$ must be of finite range and slowly varying in $\vec{q}$-space (Fig. 16). Then, the $\vec{k}$-integrations can be evaluated by taking $v(\vec{q}) = v(\vec{K}_n)$ for $|\vec{q} - \vec{K}_n| \lesssim \lambda(\vec{K}_n)$. The result is an infinite series of matrix products [33].

$$\begin{aligned} g(\vec{k}, \vec{k}'; E) = {} & G_0(\vec{k}; E)\, \delta(\vec{k} - \vec{k}') \times \\ & \times \Big[1 + v(0)\, G(\vec{k}; E) + \sum_n v(0, \vec{K}_n)\, \phi_n(\vec{k}; E)\, v(\vec{K}_n, 0)\, G_0(\vec{k}; E) \\ & + \sum_{nn'} v(0, \vec{K}_n)\, \phi_n(\vec{k}; E)\, v(\vec{K}_n, \vec{K}_{n'})\, \phi_{n'}(\vec{k}; E)\, v(\vec{K}_{n'}, 0)\, G_0(\vec{k}; E) \\ & + \ldots \Big] \end{aligned} \tag{40}$$

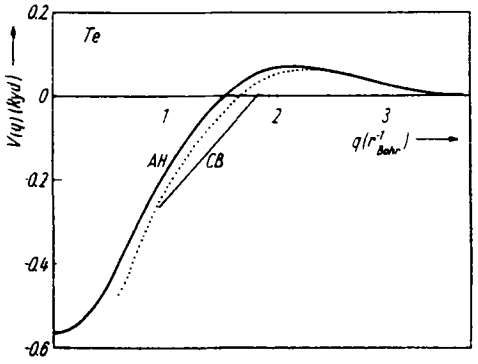

Fig. 16
Model potential of tellurium atoms in a tellurium single crystal as obtained from band structure calculations [93].

This infinite series can be summed geometrically yielding for the averaged Green's function

$$g(\vec{k}, \vec{k}'; E) = G_0(\vec{k}; E) \left[\frac{1}{1 - v\phi} \right]_{00} \delta(\vec{k} - \vec{k}') \tag{41}$$

v denotes a matraix given by

$$v_{nn'} = \frac{N}{\Omega} \int d^3 \vec{r}\, v(\vec{r})\, e^{-i(\vec{K}_n - \vec{K}_{n'})\vec{r}} \tag{42}$$

the crystalline pseudopotential matrix elements.

ϕ is a diagonal matrix with elements

$$\phi_n(\vec{k}; E^+) = \int d^3 \vec{q}\, f_n(\vec{k} - \vec{q} - \vec{K}_n) \frac{1}{E^+ - q^2} \quad . \tag{43}$$

For $\lambda \to 0$ we have $\phi_n(\vec{k}; E) = (E - (\vec{k} - \vec{K}_n)^2)^{-1}$ and equ. (41) gives the diagonal elements of the crystalline Green's function.

It is easy to generalize the procedure to a short range ordered medium consisting of clusters of atoms at the sites $\vec{a}_1 \ldots \vec{a}_m$ each cluster being situated near a lattice point $\vec{R}_l$. Instead of equ.'s (36) and (37) one has to use

$$D_n(\vec{\rho}_1 \ldots \vec{\rho}_n) = \sum_{j_1 \ldots j_n} D_2^{j_1 j_2} D_2^{j_2 j_3} \ldots D_2^{j_{n-1} j_n} \tag{44}$$

$$D_2^{jj'}(\vec{\rho}, \vec{\rho}') = \sum_l P_l(\vec{\rho} - \vec{\rho}' - \vec{R}_l - (\vec{a}_j - \vec{a}_{j'})) \,. \tag{45}$$

This yields a correct description of the molecule scattering of the atom cluster. The resulting averaged Green's function is formally the same as in equ. (41) except $v_{nn'}$ being replaced by

$$w_{nn'} = \sum_j e^{i(\vec{K}_n - \vec{K}_{n'})\vec{a}_j} v_{nn'} \tag{46}$$

the Fourier transformed potential of the atom cluster, quite analoguous to the case of a crystal with m atoms in the unit cell. The whole approach is expected to work for small disorder (well localized correlation functions) and if the pseudopotential approach works in the crystalline case.

The averaging procedure for the product of the two one electron propagators occurring in the expression (10) for the dielectric constant can be carried out quite similar

to that sketched above for the simple one-electron propagator [35]. The approximative result is

$$\epsilon_2(\omega) \sim \frac{1}{\omega^2} \int dE \int d^3\vec{k} \sum_n (\vec{e}\cdot\vec{k}) \times$$
$$\times \operatorname{Jm} g(\vec{k}, \vec{k}-\vec{K}_n; E^+)\,(\vec{e}\cdot[\vec{k}-\vec{K}_n]) \times \tag{47}$$
$$\times \operatorname{Jm} g(\vec{k}-\vec{K}_n, \vec{k}; E^+ + \omega)\; F(T; E, \omega)\,.$$

The off diagonal elements of the averaged Green's function, $g(\vec{k}, \vec{k}-\vec{K}_n; E^+)$, are given quite analoguous to equ. (41).

It is worth mentioning, that a similar ansatz for the correlation functions can be used to average the one-electron propagator by starting from the KKR-method well known from crystalline band structure calculations. Using a complex effective atomic scattering matrix one includes partly the scattering properties of the whole disordered medium in the scattering properties of one atom [11 to 13, 80].

V.2. Properties of the averaged Green's function

The only important quantity one needs to know for the discussion of the electronic properties is the imaginary part of the averaged Green's function. For a first insight it is only necessary to investigate the behaviour of the diagonal part of $\operatorname{Jm} g(E^+)$, the so called spectral function. It is useful to rewrite the averaged Green's function into a form more suitable for practical purposes using its poles in the complex energy plane and the respective residues.

$$g(\vec{k}; E^+) = \sum_m \frac{\operatorname{Res} g(\vec{k}; E^+)\big|_{E=\epsilon_m(\vec{k})}}{E^+ - \epsilon_m(\vec{k})}\,. \tag{48}$$

The poles, $\epsilon_m(\vec{k})$, are given by the roots of

$$\det |\phi_n^{-1}(\vec{k}; E)\,\delta_{nn'} - w_{nn'}| = 0\,. \tag{49}$$

For complete order, i.e. vanishing width of the localization of the Fourier transformed correlation functions, equ. (49) turns out to be the pseudopotential equation for the energy band structure of a crystalline system.

$$\det |(E - (\vec{k}-\vec{K}_n)^2)\,\delta_{nn'} - w_{nn'}| = 0\,. \tag{50}$$

The roots of equ. (50) are situated at the real energy axis due to $G_0(\vec{k}-\vec{K}_n; E)$ being real for $E \neq (\vec{k}-\vec{K}_n)^2$. Using the spectral representation (12) one derives the residues of $g(\vec{k}; E)_{\text{crystal}}$ als $|\langle\vec{k}|\psi_{m\vec{k}}\rangle|^2$.

The imaginary part of $\phi_n(\vec{k}; E)$ is nonzero and finite for $E \approx (\vec{k}-\vec{K}_n)^2$ and depends on the degree of disorder. Hence, for real $\vec{k}$ the roots of equ. (49) are located in the

complex energy plane. For small disorder, i.e. small width of the localization of the two-atom correlation function, we expect the real parts of $\epsilon_m(\vec{k})$ to be almost the same as in the crystalline case. The main effect of the relaxation of the long range order is to shift the poles of the averaged Green's function into the complex energy plane. The imaginary part of $\epsilon_m(\vec{k})$ depends on the degree of disorder. It can be interpreted physically as a reciprocal life time of a Bloch state belonging to the real part of $\epsilon_m(\vec{k})$.

The behaviour of the electronic spectrum can be studied by investigation of the spectral function in nearly free electron (NFE) approximation, i.e. for a weak potential with matrix elements

$$w_{nn'} = \begin{cases} v_1 \ll K_1^2 & \text{for } \vec{K}_n - \vec{K}_{n'} = \vec{K}_1 \\ 0 & \text{for } \vec{K}_n - \vec{K}_{n'} \neq \vec{K}_1 \end{cases} \tag{51}$$

In the crystalline case the spectral function is a delta function at $E = E_m(\vec{k})$ denoting the $\vec{k}$-dependent roots of equ. (50). The residues of $g(\vec{k}; E)_{crystal}$ giving the strengths of the delta functions are nonzero only for $E \approx k^2$, the free electron parabola. A qualitative picture of $E_m(\vec{k})$ is plotted in Fig. 17a exhibiting the spitting of the free electron parabola near $\vec{k} = \vec{K}_1/2$.

In the disordered case the spectral function is approximately a Lorentzian curve centered at $E = \mathrm{Re}\,\epsilon_m(\vec{k}) \approx E_m(\vec{k})$. The width of the Lorentzian curve is given by $\Gamma_m(\vec{k}) = \mathrm{Jm}\,\epsilon_m(\vec{k})$. $\Gamma_m(\vec{k})$ turns out to be nonzero only for $\vec{k} \approx \vec{K}_1/2$. The strength of the Lorentzian curve is given by the residue of $g(\vec{k};E)$ being nonzero only for $E \approx k^2$ as in the crystalline case. The complex band structure is shown qualitatively in Fig. 17b. The width of the shaded region is twice the imaginary part of the energy and denotes the width of the spectral function (Fig. 17c). Inspection of Fig. 17 suggests, that the main disorder effects in the density of states and the imaginary part of the dielectric constant have to be expected at energies belonging to critical points in the crystalline energy spectrum. For example, the van Hove singularities in the density of states are smoothed out by the relaxation of the long range order as pointed out qualitatively in Fig. 18. These results are essentially the same as already obtained by Edwards in 1962 by application of perturbation theory and evaluating the self energy of the system in powers of the atomic potential [81, 82]. Similar results are obtained also in the case of compositional disorder by several authors by use of somewhat different formalisms and assumptions concerning the correlation function [8, 19, 20, 83, 84].

V.3. Application to real systems

From the preceding section it is evident that a reasonable first step in calculating the electronic properties of a structurally disordered solid is the computation of the

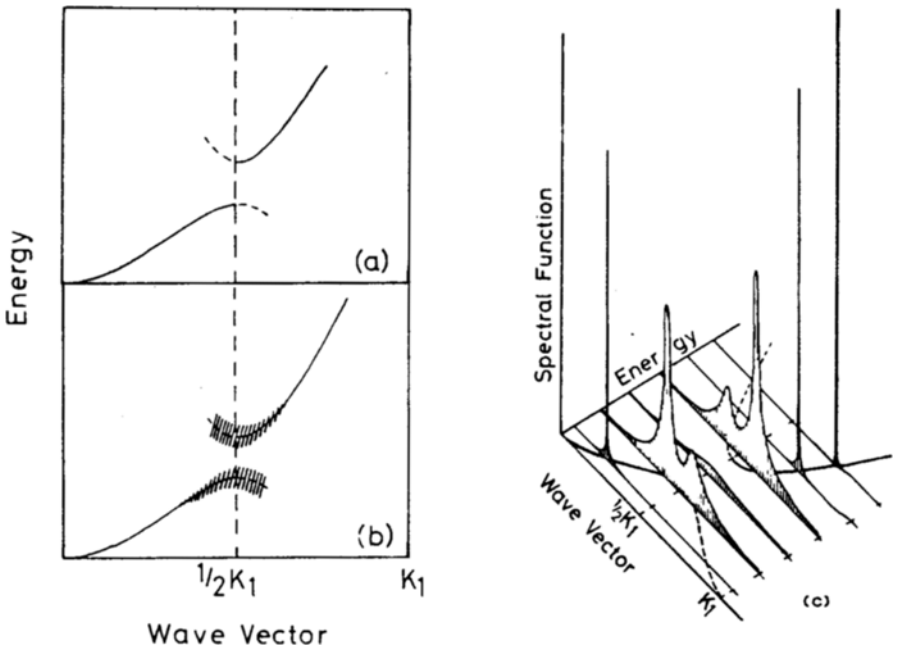

Fig. 17. a) Qualitative picture of the poles of the averaged Green's function for $\alpha = 0$ (crystal) in weak potential approximation. The splitting of the free electron parabola at the boundary of the Brillouin zone is due to long range order. b) The complex poles of the amorphous ($\alpha \neq 0$) Green's function. The real part of energy is indicated as a heavy line. The width of the shaded area denotes twice the imaginary part of the energy. The lack of long range order influences predominatly the energy spectrum near the zone boundary. c) The spectral function, Im $g(\vec{k}; E)$, in weak potential approximation. In the crystalline case ($\alpha = 0$) the imaginary part of the Green's function is a delta function at $E = E(\vec{k})$. In the amorphous case the delta function is broadened according to the imaginary part of energy. The spectral function is nonzero within the energy gap. This indicates a nonzero density of states.

complex poles of the averaged Green's function. For small disorder one may assume the residues of the Green's function to be the same as in the crystalline case. Hence, if $\epsilon_m(\vec{k})$ is almost periodically in $\vec{k}$-regions, where the residues are different from zero, we can rewrite the density of states and the imaginary part of the dielectric constant as follows

$$n(E) = -\frac{1}{\pi} \sum_m \int d^3k \, \mathrm{Jm} \, \frac{1}{E - \epsilon_m(\vec{k})} \tag{52}$$

$$\epsilon_{2\,(T=0)}(\omega) = \frac{\text{const}}{\omega^2} \int_{-\omega}^{0} dE \sum_{mm'} \int d^3k |M_{mm'}(\vec{k})|^2 \, \mathrm{Jm} \, \frac{1}{E - \epsilon_m(\vec{k})} \, \mathrm{Jm} \, \frac{1}{E + \omega - \epsilon_{m'}(\vec{k})} \tag{53}$$

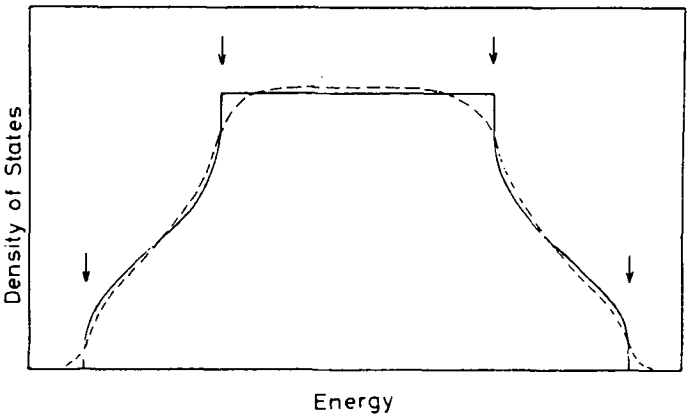

Fig. 18. Qualitative picture of the density of states as the crystalline phase is transformed into an amorphous one. Main disorder effects occur at energies near the van Hove singularities

$|M_{mm'}(\vec{k})|^2$ are the crystalline transition probabilities. For small disorder and almost $\vec{k}$-independent imaginary part of energy the expressions (52) and (53) are essentially the lifetime broadened crystalline quantities. The comparison of the calculated crystalline and amorphous band structures should give a first survey about the behaviour of the electronic properties transforming the crystalline into the amorphous structure.

For practical applications it turned out to be reasonable to choose the Fourier transformed correlation function to be a sum of Gaussians with half widths proportional to the amount of the reciprocal lattice vectors $\vec{K}_n$.

$$h_2^{jj'}(\vec{k}-\vec{q}) = \sum_{n<N_0} \frac{1}{\pi^{3/2}} \frac{1}{\alpha^3 K_n^3} e^{i\vec{K}_n(\vec{a}_j - \vec{a}_{j'})} \times e^{-\frac{(\vec{k}-\vec{q}-\vec{K}_n)^2}{\alpha^2 K_n^2}} + \sum_{n\geqslant N_0} \frac{1}{\pi^{3/2}} \frac{1}{\alpha^3 K_{N_0}^3} e^{i\vec{K}_n(\vec{a}_j - \vec{a}_{j'})} e^{-\frac{(\vec{k}-\vec{q}-\vec{K}_n)^2}{\alpha^2 K_{N_0}^2}} \tag{54}$$

$N_0 >$ dimension of the pseudopotential determinant. Then, the averaged free electron propagator can be evaluated to give a sum of error functions [36, 80]. Furthermore, it is appropriate to take the lattice constant and the unit cell of the lattice underlying the disordered structure to be the same as in the respective crystalline modification of the material. This implies the use of the same potential matrix elements as in the crystalline case.

Principally, the disorder parameter α can be determined from the experimental two-atom distribution function (see chapter II). Practically it is used as a fitting parameter. The local atomic correlation can be calculated from equ. (54) by Fourier transformation. It is

$$D_2(\vec{x}) = \delta(\vec{x}) + \sum_{(\vec{R}_l + \vec{a}_j - \vec{a}_{j'}) \neq 0} \frac{1}{\pi^{3/2}} \frac{1}{\alpha^3 x^3} e^{-\frac{(\vec{x} - (\vec{R}_l + \vec{a}_j - \vec{a}_{j'}))^2}{\alpha^2 x^2}} . \qquad (55)$$

From this we get the diameter of the short range order region, x_{SR}, by

$$x_{SR} = \frac{a_0}{2\alpha} \qquad (56)$$

a_0 = next neighbors distance.

a_0 is about 2 Å for covalent semiconductors and the measured atomic distributions exhibit bumps up to about 10 Å. Hence, α should be of the order of magnitude 10^{-1}. As an example, Fig. 19 shows the atom distribution of Ge calculated according to equ. (55) for different values of α. The comparison with the experimental curve shows, that it is not possible to reproduce the vanishing of the peak belonging to third neighbors. This is due to the assumption that the half widths of the Gaussians are linear in $\vec{K}_n$. Up to now, complex band structure calculations have been performed for Ge, Si, the III–V compounds, Se, and Te. The results are plotted in Fig.'s 21 to 34.

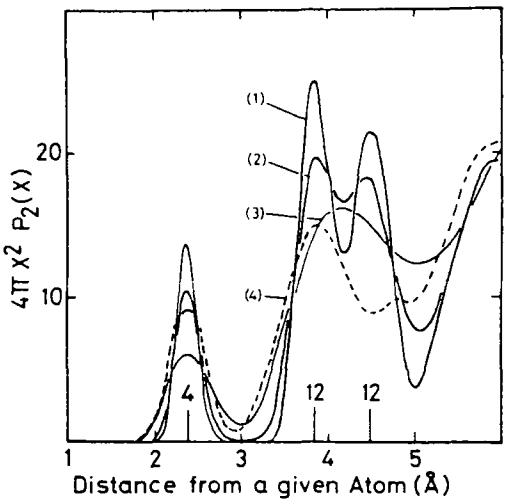

Fig. 19
Calculated radial atomic distribution functions of germanium.
1. $\alpha = 0.07$
2. $\alpha = 0.09$
3. $\alpha = 0.12$
4. experiment

VI. Discussion of results

VI.1. Tetrahedrally bonded semiconductors

From the tight binding approach discussed in chapter IV.1 we found the existence of an energy gap to be determined only by the presence of *perfect* short range order. Using the model Hamiltonian (18) one obtains in general two bands (Fig. 9). The uppermost is pure antibonding for $V_1/V_2 < 1/2$ and pure p-like for $V_1/V_2 > 1/2$. The lower band turned out to be pure bonding for $V_1/V_2 < 1/2$ and pure s-like for $V_1/V_2 > 1/2$. For $V_1/V_2 < 1/2$ the high energy edges of both bands correspond with pure p-like states that are of bonding character for the lower band and of antibonding character for the higher band (Fig. 10). These band edges belong to delta functions of weight unity in the density of states (Fig. 11). For $V_1/V_2 > 1/2$ the delta functions are situated at the upper and lower edges of the higher (p-like) band. Deviations from the perfect short range order are equivalent to a certain amount of compositional disorder. So, these statements are in agreement with other investigations yielding a tailing of the density of states into the gap region for compositionally disordered systems [e.g. 8, 16, 83, 84]. Structural investigations concerning the possibility of constructing random networks [69 to 71] show that it is impossible to construct an *infinite* random network *without* allowing for *stretching* and *bending* of bonds. Hence, we must conclude that for real amorphous systems the density of states is nonzero for all energies. The density of states may, however, exhibit "pseudogaps": energy regions with almost vanishing density of states. Therefore, these tight binding results are not in contradiction to the experiments that show clearly the existence of states within the gap.

Statements about the disorder behaviour of the electronic spectrum can be made by considering two extremal cases: The crystalline tetrahedrally coordinated structure is perfectly long range ordered. The Bethe lattice contains all possible tetrahedrally coordinated structures. Therefore, from the comparison of the respective densities of states (Fig. 11 bottom) one may conclude that only the highest valence band is due to short range order. The deeper bands and the conduction bands are mainly determined by long range order. This argument gets support by photoemission and x-ray emission data obtained for Ge and Si by various groups [49 to 51, 43]. These data show clearly the conservation of the gross shape of the upper valence band in the amorphous phase compared with the crystalline phase (see also Fig. 2).

At first sight, this result may be regarded as confirmed also by optical absorption measurements. The amorphous ϵ_2-curve of Fig. 1 can be interpreted as showing a conservation of the low energy edge of the absorption spectrum. However, the width of the upper valence band is about 4 eV, the width of the absorption curve is about 4 eV, too. Hence, the higher absorption peaks (E_2 and E_1' in Fig. 1) being more decreased by disorder than the peak E_1 originate also in transitions from the upper-

most valence band. Therefore, in order to explain the different structure dependence of various parts of the optical spectrum, we need information about the *structure dependence* not only of the diverse energy bands but also of the *different parts* of one band.

Just this missing information one obtains from the pseudopotential approach described in the preceeding chapter. The main features of the electronic spectra can be compiled as follows (Fig.'s 21 and 27):

(a) the imaginary parts of energies in the valence bands are smaller than those of energies in the conduction band.

(b) The imaginary parts of energies at the valence band edge near the axix $\Gamma - L$ (Fig. 20) are smaller than near point X.
The same holds for the conduction band edge.

(c) The imaginary parts of energies in the higher conduction bands near $\Gamma - L$ are larger compared with those belonging to the conduction band edge.

The almost vanishing imaginary parts of energies in the valence band cause a conservation of the valence band density of states, when the crystalline phase is transformed into the amorphous phase (Fig. 22). The conduction band is smeared out almost completely. Due to the rather small imaginary parts of energies near the Γ–L–axis, we observe a conservation of the higher energetic parts of the valence band and the lower energetic parts of the conduction band density of states. The deeper, respectively higher, structures are smoothed out with increasing disorder.

Inspection of the photoemission data (Fig. 2) confirms this result. The structures (2), (3) correspond with the deeper parts of the uppermost valence band and are much more affected by the lack of long range order. We may interprete the low energy edge of the conduction band as well as the high energy edge of the valence band as determined by the short range order. Interesting to note that the respective

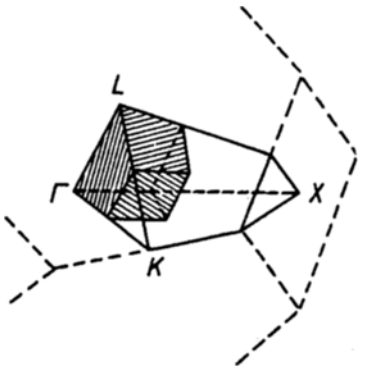

Fig. 20
Irreducible part of the Brillouin zone of Ge, Si, and the III-V compounds. The shaded part denotes the $\vec{k}$-region, where transitions contributing to E_1 and E_1' of the crystalline ϵ_2-spectrum originate

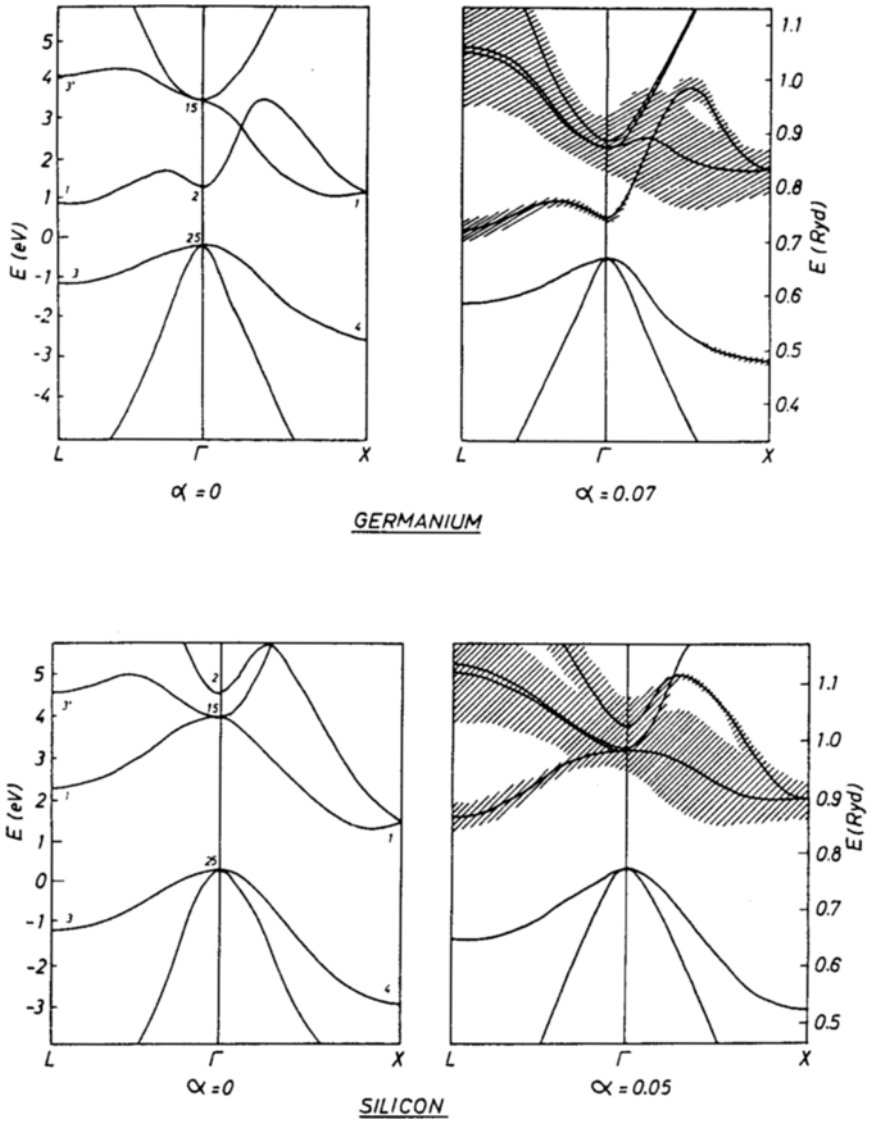

Fig. 21. Complex band structures of germanium and silicon. Full lines: real parts of energies, widths of the shaded regions: twice the imaginary part of the energy [36]

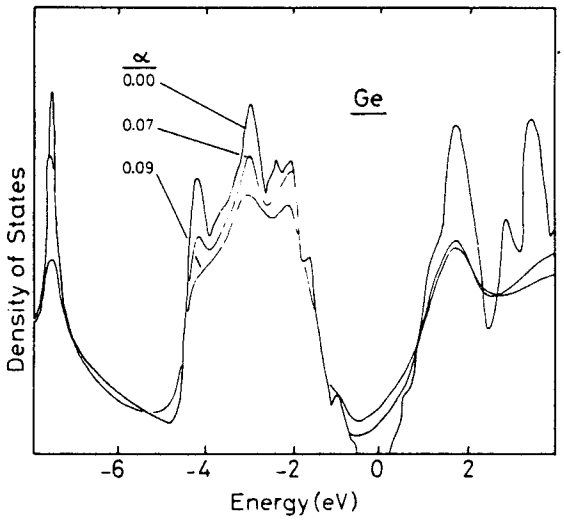

Fig. 22
Density of states of germanium calculated for various values of the disorder parameter. The lower parts of the valence band and the higher parts of the conduction band are more influenced by disorder than the band edges.

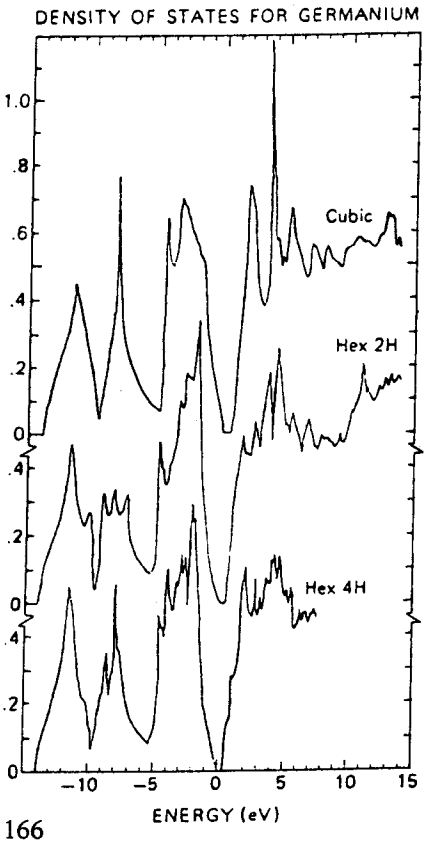

Fig. 23
Calculated densities of states for three polytypes of crystalline germanium. The cubic structure contains only staggered configurations. The 2H structure if one looks down the c-axis is eclipsed but staggered perpendicular to c-axis. In the 4H structure there are alternate layers of cubic and hexagonal neighborhoods [88].

complex energies belong to $\vec{k}$-vectors near the (111) axis. It can be considered as being preserved in the amorphous phase (see also Fig. 8), since it coincides with the directions of the bonds.

Quite another way of studying the long range order dependence of the electronic properties is to calculate the density of states or the ϵ_2-spectrum of crystals exhibiting the same short range order but a different long range order. Those calculations have been performed for various modifications of Ge, namely cubic Ge and hexagonal polytypes [88]. The results for the density of states are plotted in Fig. 23. The high energy edge of the upper valence band as well as the conduction band edge are not at all influenced by the variations in long range order. These results are an excellent confirmation of the statements we made above.

The optical spectra of the amorphous tetrahedrally coordinated semiconductors are well described by the non direct transition model (Fig. 14). The good agreement between experiment and theory is, particularly in the case of Si, a consequence of the indirect gap between Γ and X. It is this indirect gap that causes the shift in the whole spectrum to lower energies.

Details about the disorder behaviour of the different peaks in the ϵ_2-spectrum can be obtained from the pseudopotential approach. The low energy peak E_1 is due to transitions from the valence band edge to the conduction band edge near the Γ-L-axis. E_2 can be assigned to transitions near point X, $E_{1'}$ originates in transitions from the valence band to the higher conduction bands near the Γ-L-axis. Considering the complex band structures we note that with increasing α the peaks E_2 and $E_{1'}$ must be decreased much more because of the rather large imaginary parts of energies in the respective $\vec{k}$- and E-regions (Fig. 24).

Comparing the experimental ϵ_2-spectra with those calculated by using the pseudopotential approach (Fig.'s 25 and 28), one observes at least a good qualitative agreement for the higher energetic parts of the curves. The disagreement at photon energies near the absorption edge is due to a rather crude approximation involved in the actual calculations. The spectra are computed by lifetime broadening the crystalline combined density of states. Brust's calculation [86, 87] of the ϵ_2-spectrum of amorphous Ge (Fig. 26a, dotted line) shows that one obtains quantitatively better results using the more correct equ. (53). From the present approximative calculations we have the interesting point that the absorption spectra of amorphous Ge, Si and the III–V compounds can be explained by a selective, disorder dependent decrease of the higher energetic peaks of the crystalline spectra. This means that E_2 and $E_{1'}$ are predominantly determined by the long range order. E_1, however, is due to short range order. This conclusion is also confirmed by the calculations on the different modifications of crystalline Ge (Fig. 26).

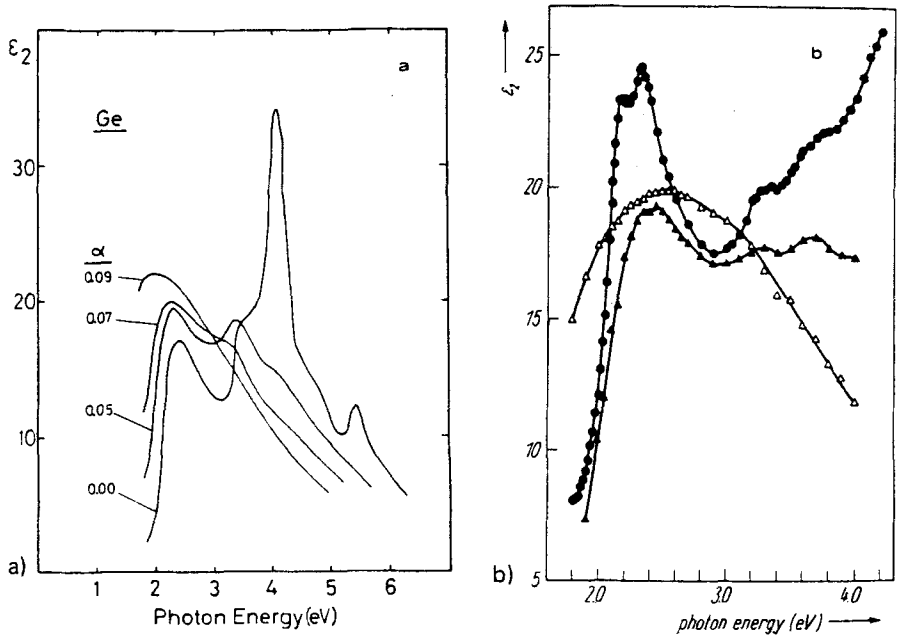

Fig. 24. ϵ_2-spectrum of germanium a) calculated for different disorder parameters, and b) as obtained form the experiment (Δ 200 °C, ▲ 300 °C substrate temperature, • single crystal) [41]. The lower part of the spectrum is short range order determined.

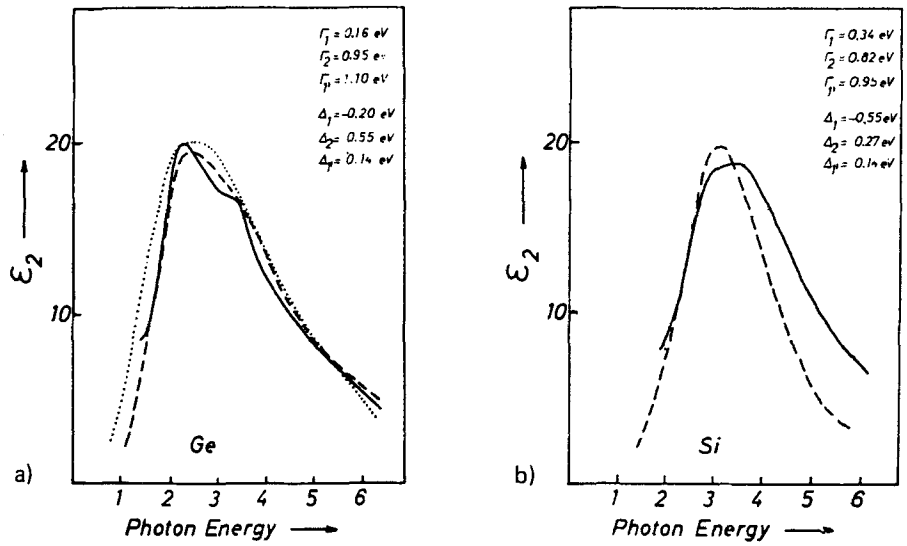

Fig. 25. ϵ_2-spectra of a) germanium, b) silicon [36]. Solid line: calculated by using the complex band structure approach, dashed line: experimental curve, dotted line: as calculated by Brust [86].

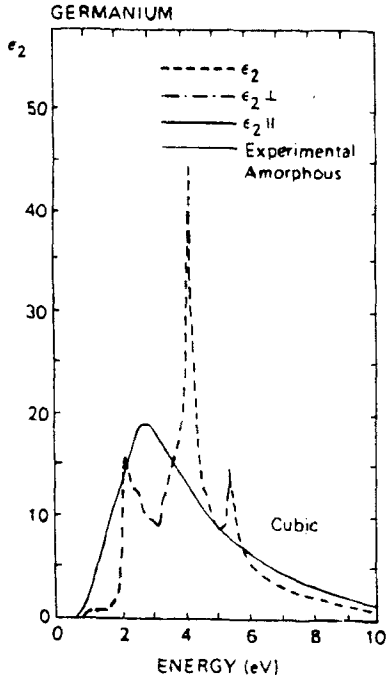

Fig. 26
ϵ_2-spectra of polytypes of crystalline germanium [88]

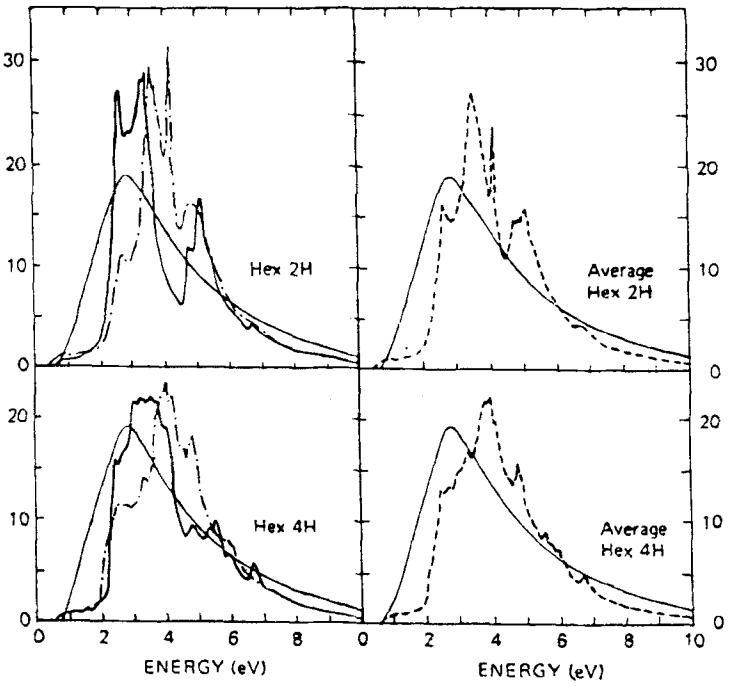

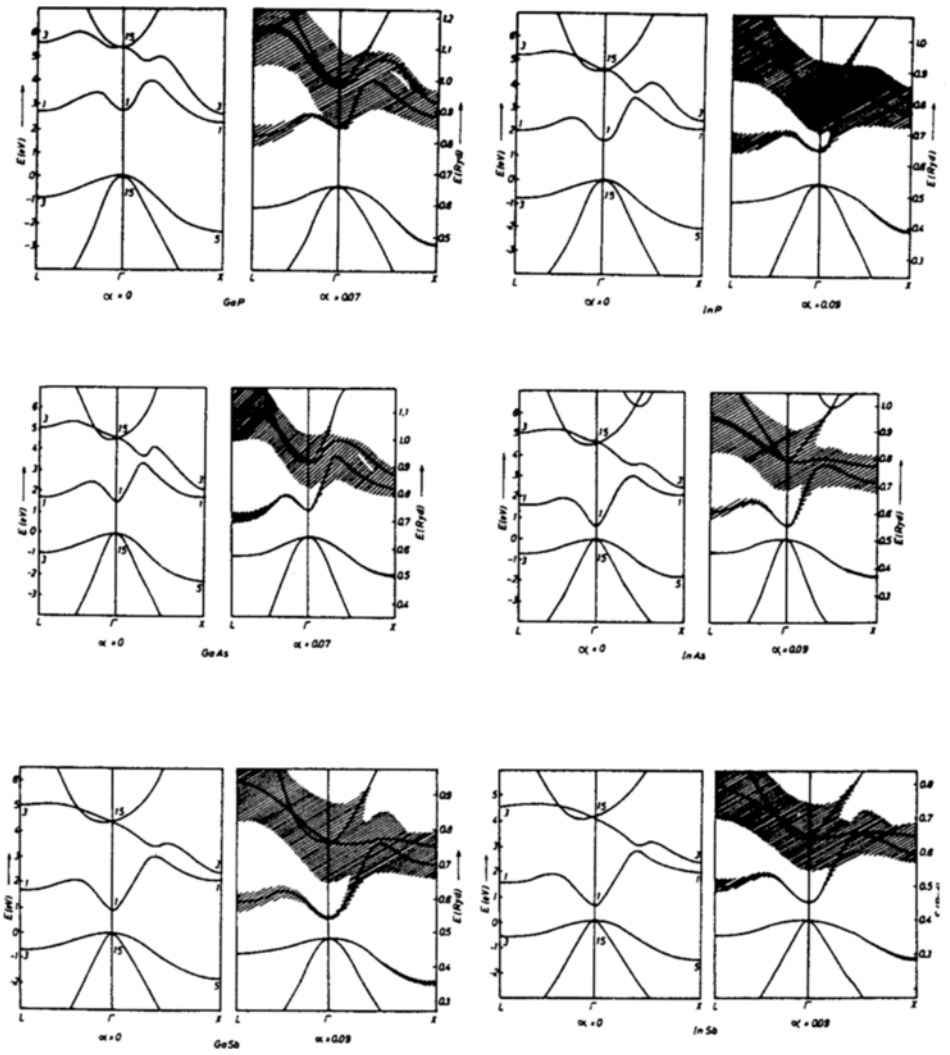

Fig. 27. Complex band structures of the III-V compounds [37].

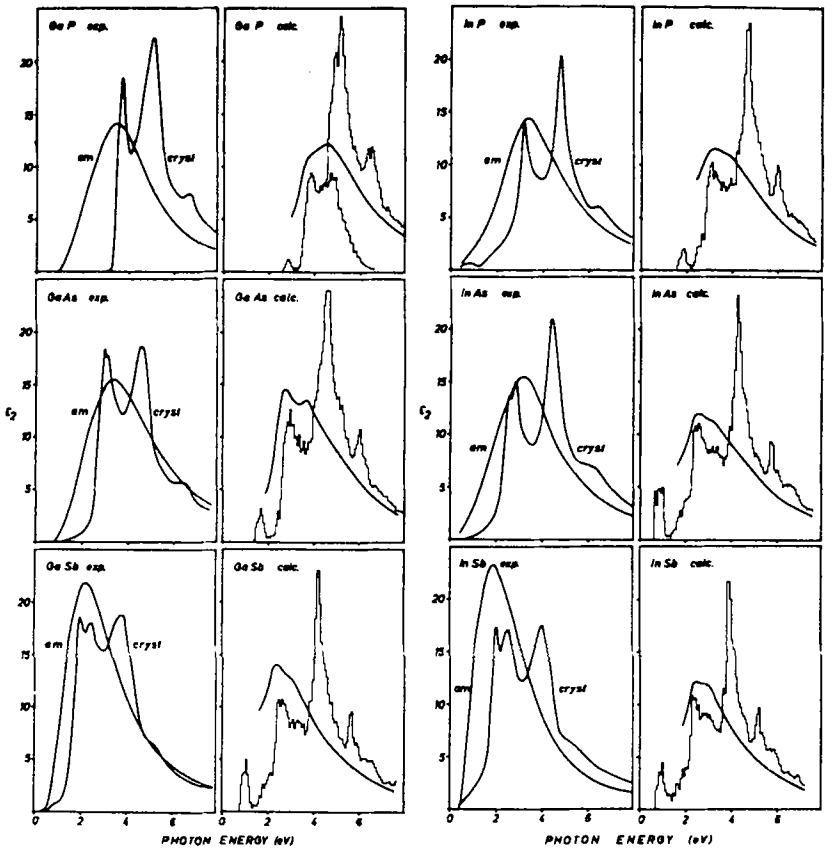

Fig. 28. ϵ_2-spectra of the III-V compounds. Left hand side: experiment, right hand side: as calculated by using the complex band structures of Fig. 27 [38]

VI.2. Selenium and Tellurium

Qualitatively similar results one finds for the elemental semiconductors Se and Te. The complex band structures in Fig.'s 30 and 33 show small imaginary parts of energies near the Δ-axis at least for the highest valence band triplet and the lowest conduction band triplet. The imaginary parts of energies in the valence bands are smaller than those of energies in the conduction bands. In the case of Se the lower

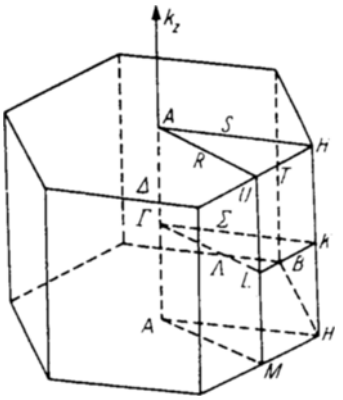

Fig. 29
Brillouin zone of trigonal selenium and tellurium.

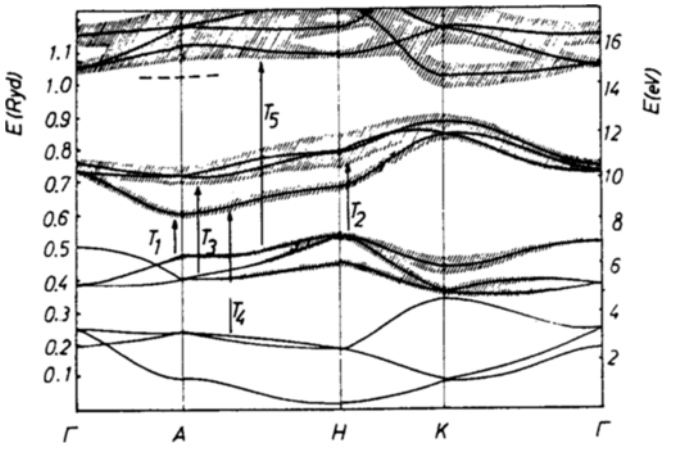

Fig. 30. Complex band structure of selenium. The arrows labelled by $T_1 \ldots T_5$ denote transitions contributing to different structures in the ϵ_2-spectrum of crystalline Se [35].

edge of the second conduction band exhibits small imaginary parts of energy. This gives rise for a bump occuring in the respective density of states (Fig. 31a). On the other side the second conduction band of the density of states of Te (Fig. 34a) is completely smoothed out because the respective imaginary parts of energies are about one order of magnitude larger than for the lower conduction band. Hence, in Se and Te the short range order dependent parts of the electronic spectrum are the three bands denoted by p_1, p_2, and p_3 in Fig.'s 30 and 33. The energy gap, situated between p_2 and p_3, is well preserved in the amorphous phases. Within the three lower triplets the contribution from a $\vec{k}$-region near the Δ-axis is more short range order determined than the contributions from other parts of the $\vec{k}$-space. Again, we

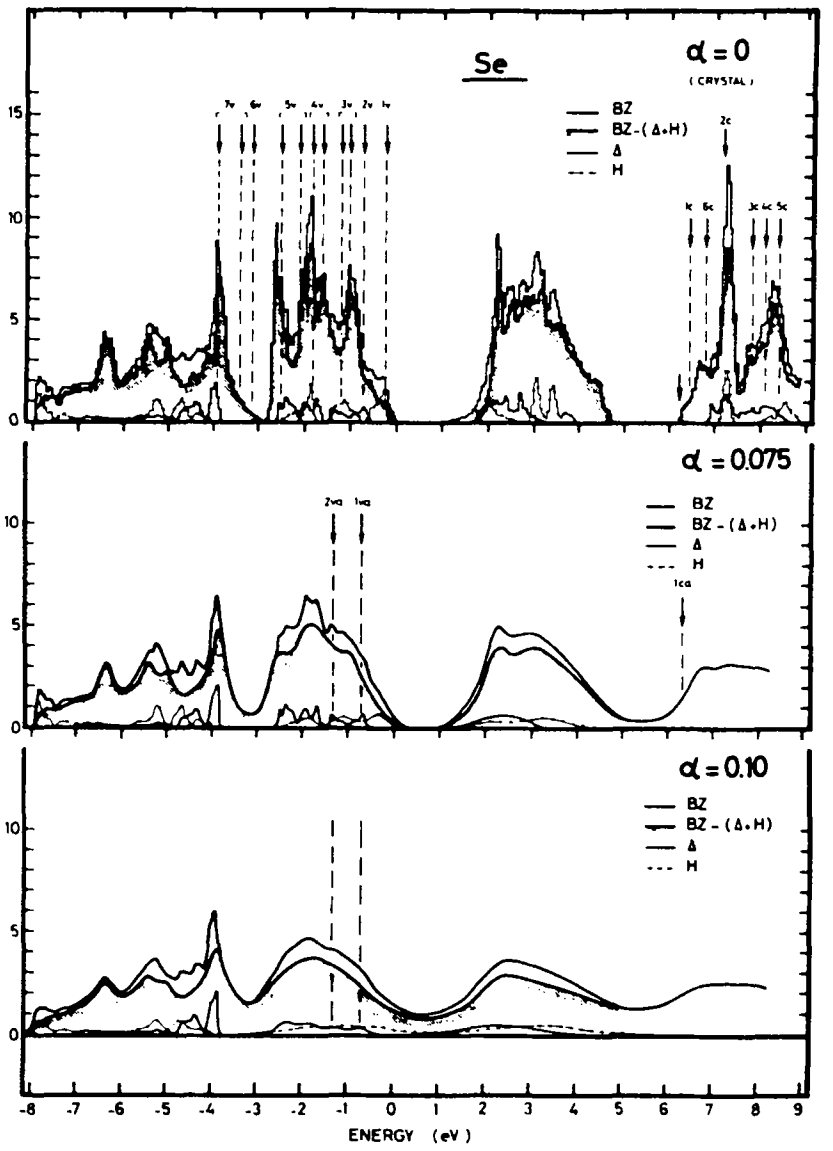

Fig. 31. a) Density of states of selenium [46, 48]. The arrows denote positions of structures in the density of states as resulting from high resolution photoemission measurements (see Fig. 31b).

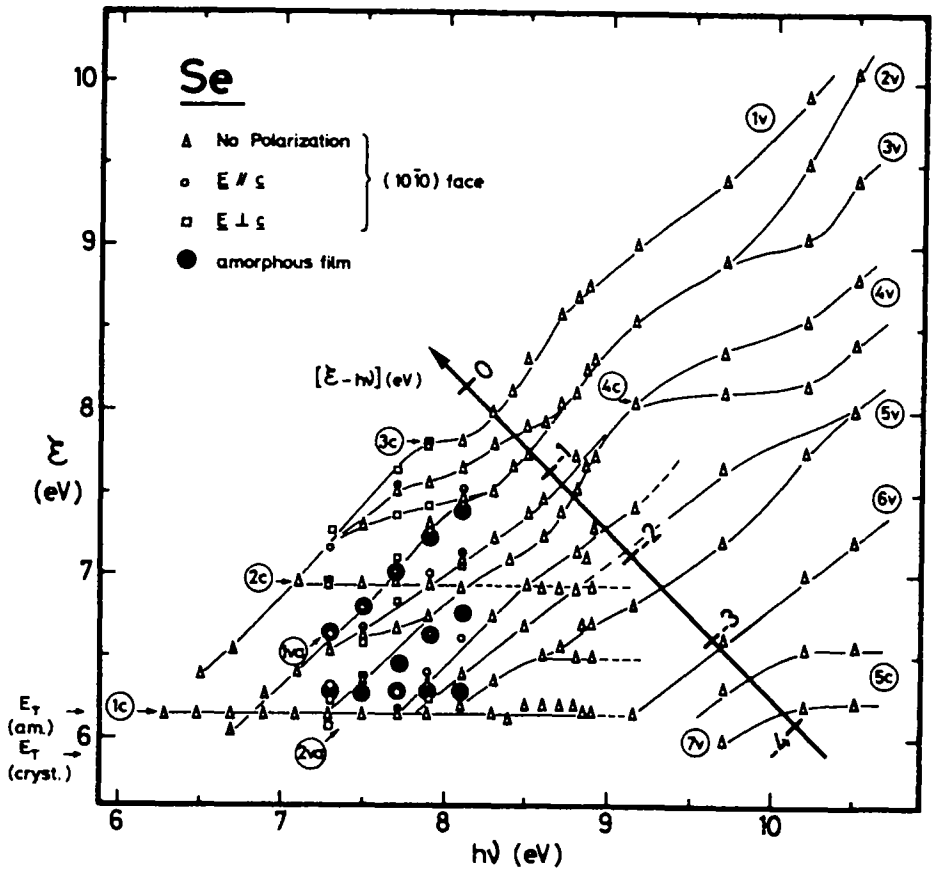

Fig. 31. b) Energy diagram of selenium [46, 48]. The energetic positions of peaks in the third derivatives of the photocurrent are indicated as triangles, rectangles, and circles in the crystalline case, and as black dots in the amorphous case. Structures stable in final energy, $\mathscr{E}$, can be assigned to conduction band features, structures stable in the initial energy, $\mathscr{E} - \hbar\omega$, are connected with valence band features.

state a conservation of the energy spectrum along the preferential direction of the short range order.

Experimentally one can study the fine structure of the density of states tracing the EDC-curves of photoemitted electrons with photon energy. Fig. 31c shows EDC-curves of amorphous Se belonging to various photon energies [44]. The shape of the curves verifies qualitatively the calculated valence band density of states. One gets more accurate information by improving the resolution with modulation techniques [45 to 48]. Structures in the EDC-curves that are stable in the final energy, $\mathscr{E}$, can

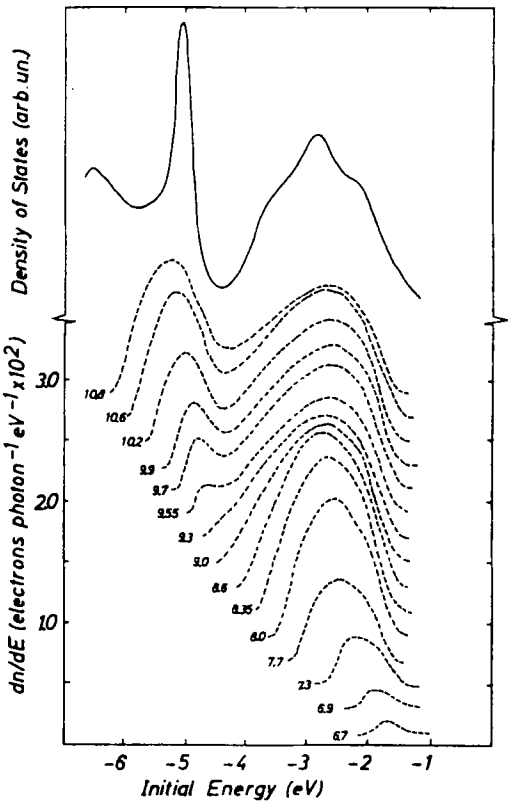

Fig. 31

c) Experimental EDC – curves of amorphous Se for various photon energies. The uppermost curve is the calculated valence band density of states [44]

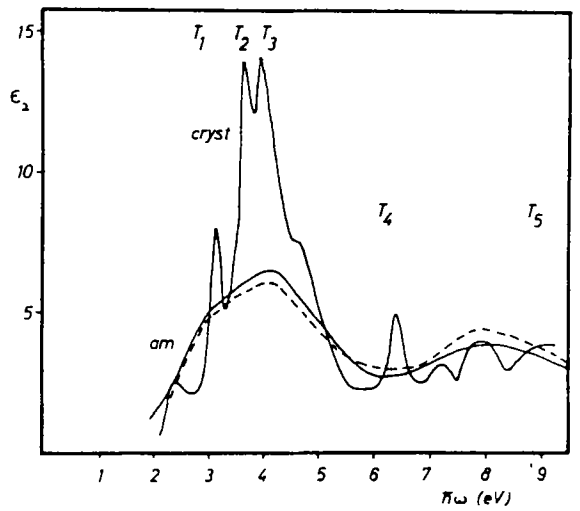

Fig. 32

ϵ_2-spectrum of selenium [35]. Crystalline case: isotropic average based on the calculation of Sandrock [95]. Amorphous case: full line: calculated by using the complex band structure, dashed line: experimental curve [96].

be assigned to conduction band features. Structures stable in the initial energy, $\mathcal{E} - \hbar\omega$, correspond with valence band features. The energy diagram, containing the behaviour of all the peaks and bumps of the EDC-curves, yields the information about the electronic density of states. Two examples are given in Fig.'s 31b and 34b for crystalline and amorphous Se and Te. The comparison of the energy diagrams and the calculated electronic spectra shows a rather satisfying agreement between experiment and theory.

The low energy part of the ϵ_2-spectrum of trigonal Se consists of three peaks T_1 ... T_3 (Fig. 32). The first is due to transitions from the valence band edge to the conduction band edge in a region near point A of the Brillouin zone (Fig. 29).

Inspection of the complex band structure (Fig. 30) shows that just for these transitions the imaginary parts of energies are smaller than those belonging to higher energetic transitions. Therefore, a considerable amount of T_1 is determined by short range order, whereas T_2 and T_3 are more influenced by the long range order. Consequently, the amorphous ϵ_2-spectrum is expected to show at least a bump at photon energies near T_1. This is confirmed by a comparison of the calculated and the experimental spectrum (Fig. 32).

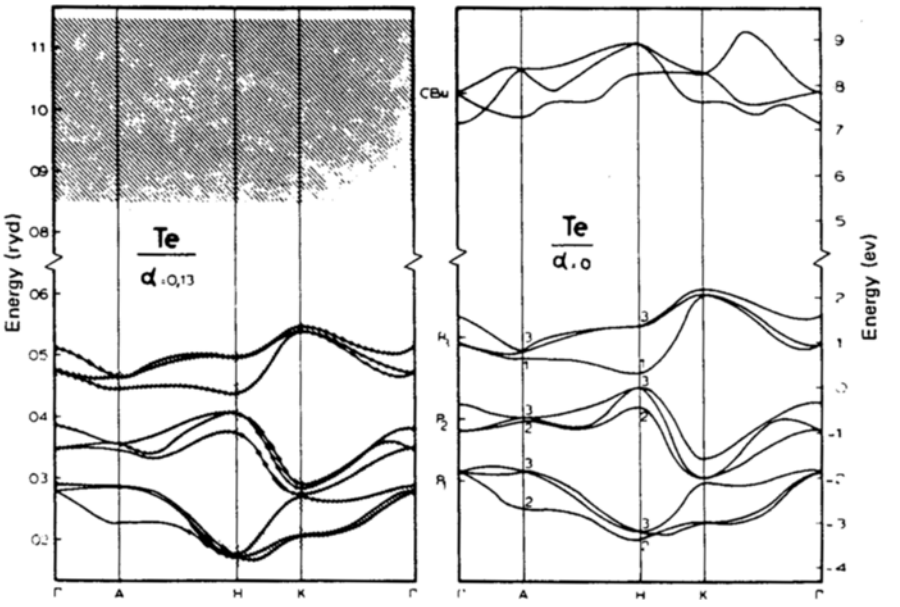

Fig. 33. Complex band structure of tellurium [48]. The imaginary parts of energy in the second conduction band (CBu) are one order of magnitude larger than those in the lower bands p_1, p_2, p_3. Therefore, this triplet is indicated in the amorphous case as a shaded area.

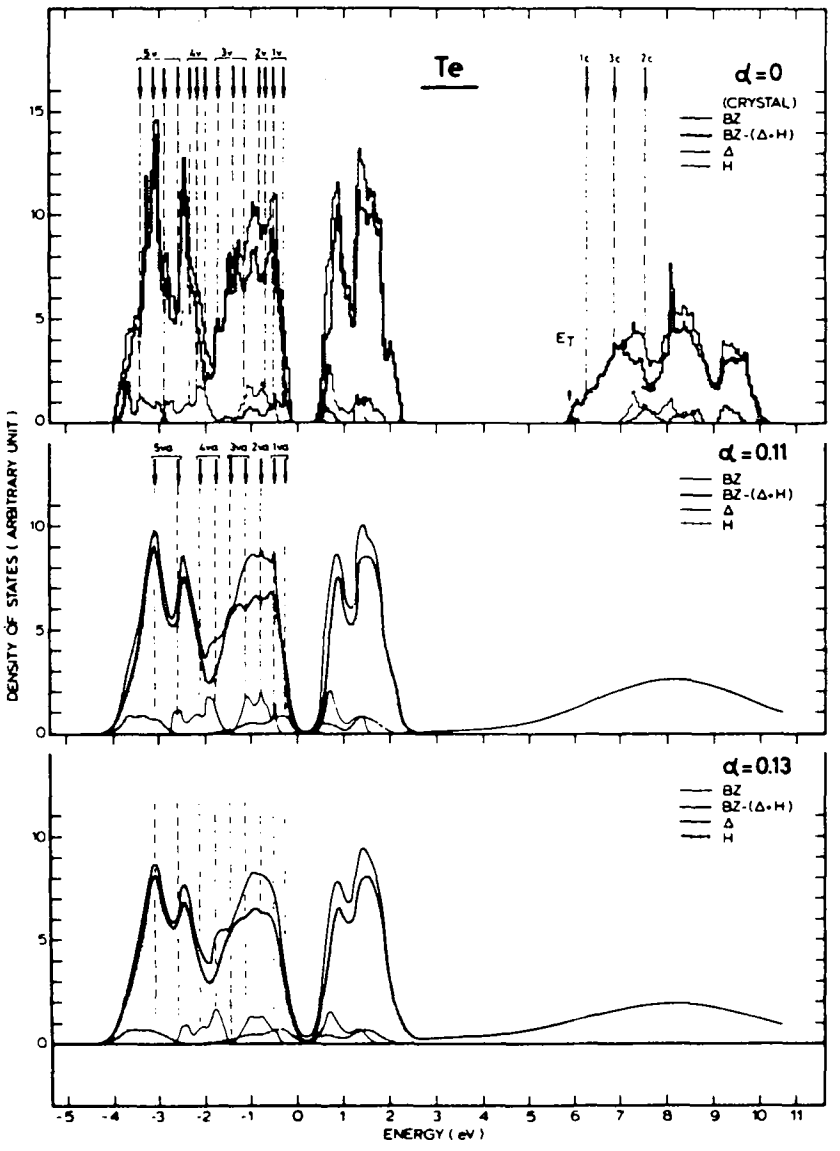

Fig. 34. a) The density of states for tellurium [48]. The arrows denote energetic positions of structures as coming out of the experiment (Fig. 34 b).

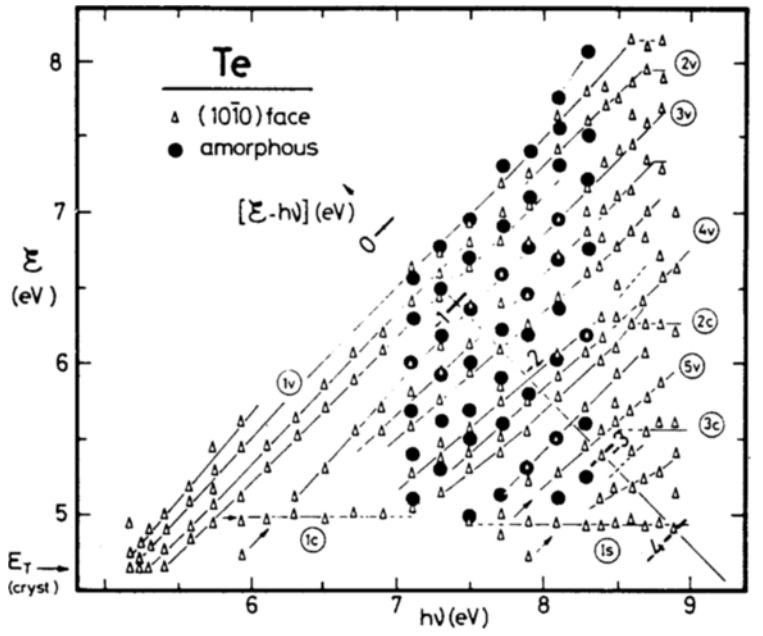

Fig. 34. b) Energy diagram of tellurium as obtained from high resolution photoemission measurements.

Conclusions

Summarizing we state that the methods described in chapters IV and V allow a satisfying description at least of electronic properties connected with states well within energy bands. To investigate the structure dependence of those properties we introduced the structural characteristics "short range order" and "long range order". This gave rise for the possibility of discussing the electronic density of states and the optical absorption without referring to details of the structure, i.e., provided a given short range order, it was not necessary to know, *how* the long range order was relaxed.

In the last chapter we discussed the electronic spectrum by making extensive use of the disorder behaviour of the poles of the configurationally averaged Green's function. These are relatively easy to calculate and save the evaluation of the full Green's function. From the standpoint of application it is this complex energy scheme that is the most important result of the preceeding considerations.

To study the disorder behaviour of the band edges one has to investigate the effect of fluctuations in the short range order. In the tight binding case, this can be done by calculating overlap integrals including variations in bond angles and lengths [89]. Principally, since the wave functions enter explicitely into the theory, one should obtain from this also information about localized states, mobility edges, etc. needed for the explanation of transport phenomena. In the pseudopotential approach small fluctuations in the short range order are included in the atomic distribution function. One obtains states in the gap automatically. Their distribution is given by the superposition of the tails in the spectral function. The number of these states, however, seems to be one order of magnitude too large. This might be due to the partial neglection of the multiple scattering terms in the Born series.

Attempts have been made in the literature to calculate the optical spectra of amorphous systems near the absorption edge. The result is an exponential absorption tail [90]. This seems to be confirmed by experimental data [58]. Averaging the product of the two one-electron Green's function one can show, that in amorphous systems an effective electron hole interaction occurs caused by the correlation between the atoms. This additional electron hole interaction is repulsive and reduces the absorption curve near the threshold [91, 92]. So, the correct treatment of the absorption edge requests the consideration of Coulombic electron hole interaction besides performing correctly the configurational average.

Acknowledgements: The author wishes to thank Prof. J. Treusch and Dr. K. Maschke for helpful discussions. The technical assistance of Miss A. Meckler and Miss U. Nutt, who prepared the paper for publication, is gratefully acknowledged.

References

[1] *H. Fritzsche* and *S. R. Ovshinsky*, J. Non.-Cryst. Sol. 4, 464 (1970).

[2] *P. W. Anderson*, Phys. Rev. 109, 1492 (1958).

[3] *L. Banyai*, Physique des Semiconducteurs (ed. M. Hulin) Dunod, Paris, 417 (1964).

[4] *M. H. Cohen*, J. Non.-Cryst. Sol. 4, 391 (1970).

[5] *N. F. Mott*, Adv. in Sol. State Phys. 9, 22 (1969) Pergamon Press Oxford.

[6] *W. Brenig*, Adv. in Sol. State Phys. 11, 175 (1971) Pergamon Press Oxford.

[7] *N. F. Mott* and *Davis*, Electronic Processes in Noncrystalline Materials (Oxford University Press, Ely House, London W. 1 (1971).

[8] *I. M. Lifshitz*, Adv. in Phys. 13, 483 (1964).

[9] *F. Yonezawa* and *T. Matsubara*, Progr. Theor. Phys. 35, 357 (1966).

[10] *F. Yonezawa* and *T. Matsubara*, Progr. Theor. Phys. 35, 759 (1966).

[11] *J. M. Ziman*, Proc. Roy. Soc. 88, 387 (1966).

[12] *P. Lloyd*, Proc. Roy. Soc. 90, 207 (1967).

[13] *P. Lloyd*, Proc. Roy. Soc. 90, 217 (1967).

[14] *R. Jones*, *T. Lukes*, Proc. Roy. Soc. A 309, 457 (1969).

[15] *J. L. Beeby*, Proc. Roy. Soc. A 279, 82 (1964).

[16] *P. Soven*, Phys. Rev. 156, 809 (1967).

[17] *B. Velický*, *S. Kirkpatrick*, *H. Ehrenreich*, Phys. Rev. 175, 747 (1968).

[18] *Y. Onodera*, *Y. Toyozawa*, J. of Phys. Soc. Japan 24, 341 (1968).

[19] *P. Soven*, Phys. Rev. 178, 9936 (1969).

[20] *D. Stroud* and *H. Ehrenreich*, Phys. Rev. B 2, 3197 (1970).

[21] *K. Levin*, *B. Velicky*, *H. Ehrenreich*, Phys. Rev. B 2 1771 (1970).

[22] *B. L. Gyorffy*, Phys. Rev. B 1, 3290 (1970).

[23] *K. S. Dy*, *Shi-Yu Wu*, Phys. Rev. B 3, 1173 (1971).

[24] *K. F. Feed*, *M. H. Cohen*, Phys. Rev. B 3, 3400 (1971).

[25] *V. Capek*, phys. stat. sol (b) 43, 61 (1971).

[26] *E-Ni Foo* and *H. Amar*, Phys. Rev. Lett. 26, 1748 (1971).

[27] *L. Schwartz* and *H. Ehrenreich*, Ann. of Phys. 64, 100 (1971).

[28] *D. Weaire*, Phys. Rev. Lett. 26, 1541 (1971).

[29] *D. Weaire*, *M. F. Thorpe*, Phys. Rev. B 4, 2508 (1971).

[30] *M. F. Thorpe*, *D. Weaire*, Phys. Rev. B 4, 3518 (1971).

[31] *D. Weaire*, *M. F. Thorpe*, Int. Conf. Am. Liqu. Semicond., Aug. 1971, Ann Arbour (Mich.) to be published in J. Non-Cryst. Sol.

[32] *M. F. Thorpe*, *D. Weaire*, Phys. Rev. Lett. 27, 1581 (1971).

[33] *B. Kramer*, phys. stat. sol. 41, 649 (1970).

[34] *B. Kramer*, *K. Maschke*, *P. Thomas*, *J. Treusch*, Phys. Rev. Lett. 25, 1020 (1970).

[35] *B. Kramer*, phys. stat. sol. 41, 725 (1970).

[36] *B. Kramer*, phys. stat. sol. 47, 501 (1971).

[37] *B. Kramer*, *K. Maschke*, *P. Thomas*, phys. stat. sol. 48, 635 (1971).

[38] *B. Kramer*, *K. Maschke*, *P. Thomas*, phys. stat. sol. 49, 525 (1972).

[39] *M. H. Brodsky, R. S. Title, K. Weiser, G. D. Pettit,* Phys. Rev. B **1**, 2632 (1970).
[40] *T. M. Donovan, W. E. Spicer, J. M. Bennett, E. J. Ashley,* Phys. Rev. B **2**, 397 (1970).
[41] *G. Jungk,* phys. stat. sol. **44**, 239 (1971).
[42] *J. Stuke, G. Zimmerer,* phys. stat. sol. **49**, 513 (1972).
[43] *G. Wiech, E. Zöpf,* to be published in Proc. Int. Conf. Band Struct. Spectr. Met. All. University of Strathclyde, Glasgow, Sept. (1971).
[44] *P. Nielsen,* Bull. Am. Phys. Soc. **16**, 349 (1971).
[45] *L. D. Laude, B. Fitton, M. Anderegg,* Phys. Rev. Lett. **26**, 637 (1971).
[46] *L. D. Laude, B. Fitton, B. Kramer, K. Maschke,* Phys. Rev. Lett. **27**, 1053 (1971).
[47] *L. D. Laude, B. Fitton,* Int. Conf. Am. Liqu. Semicond., Aug. 1971, Ann Arbour (Mich.) to be published in J. Non-Cryst. Sol.
[48] *L. D. Laude, B. Fitton, B. Kramer, K. Maschke,* to be published
[49] *T. M. Donovan, W. E. Spicer,* Phys. Rev. Lett. **21**, 1572 (1968).
[50] *W. E. Spicer, T. M. Donovan,* Phys. Rev. Lett. **24**, 595 (1970).
[51] *C. W. Peterson, J. H. Dinan, T. E. Fisher,* Phys. Rev. Lett. **25**, 851 (1970).
[52] *H. R. Philipp, H. Ehrenreich,* Phys. Rev. **129**, 1550 (1963).
[53] *J. Tauc* et al., Proc. Int. Conf. Phys. Non-Cryst. Sol., Delft, The Netherlands (1964) (North Holl. Pub. Comp. Amsterdam 1965) p. 606.
[54] *J. Stuke,* Adv. Sol. State Phys. **9**, 46 (1969) Pergamon Press, Oxford.
[55] *W. E. Spicer, R. E. Eden,* Proc. IX Int. Conf. Phys. Sem. Moscow (1968) **1**, 65.
[56] *U. Gerhard,* Adv. Sol. State Phys. **10**, 175 (1970) Pergamon Press, Oxford.
[57] *J. Tauc, A. Menth, D. L. Wood,* Phys. Rev. Lett. **25**, 749 (1970).
[58] *J. Tauc, A. Menth,* Int. Conf. Am. Liqu. Semicond., Aug. 1971, Ann Arbour (Mich.) to be published in J. Non-Cryst. Sol.
[59] *R. E. Smith,* Int. Conf. Am. Liqu. Semicond., Aug. 1971, Ann Arbour (Mich.) to be published in J. Non-Cryst. Sol.
[60] *W. E. Spear, P. G. Le Comber,* Int. Conf. Am. Liqu. Semicond., Aug. 1971, Ann Arbour (Mich.) to be published in J. Non-Cryst. Sol.
[61] *H. Krebs,* Adv. Sol. State Phys. **9**, 1 (1969) Pergamon Press, Oxford.
[62] *C. H. Griffith* and *H. Sang,* Proc. Int. Symp. Se, Te, Montreal Oct. 1967 (Pergamon Press 1969), 135.
[63] *C. Kittel,* Intr. to Sol. State Phys. (J. Wiley and Sons. Inc. London, New York, Sidney, 1966).
[64] *H. Richter, G. Breitling,* Z. Naturf. **13a**, 988 (1958).
[65] *S. C. Moss, J. F. Gradzyk,* Proc. 10th Int. Conf. Phys. Semicond. Natl. B Standards U.S. Dep. Comm. Springfield, Virginia (1970), p. 658.
[66] *N. J. Shevchik* and *W. Paul,* Int. Conf. Am. Liqu. Semicond., Aug. 1971, Ann Arbour (Mich.) to be published in J. Non-Cryst. Sol.
[67] *R. Kaplov, T. A. Rowe, B. L. Averbach,* Phys. Rev. **168**, 1068 (1968).
[68] *H. Richter, G. Breitling,* Z. Naturf. **26a**, 1699 (1971).
[69] *R. Grigorovici, R. Mănăilă,* Thin Sol. Films **1**, 343 (1967/68).
[70] *R. Grigorovici,* J. Non-Cryst. Sol. **4**, 27 (1970).
[71] *D. E. Polk,* J. Non-Cryst. Sol. **5**, 365 (1971).

[72] *A. I. Gubanov,* phys. stat. sol. 17, 807 (1966)

[73] *A. I. Gubanov,* Sov. Phys. Sol. State 7, 2547 (1966)

[74] *E. De Dycker, P. Phariseau,* Physica 34, 325 (1967).

[75] *J. Tauc,* Optical Properties of Non-crystalline Solids (to be published in Optical Properties of Solids F. Abeles North Holl. Amsterdam)

[76] *K. Maschke,* Thesis Marburg (1969).

[77] *K. Maschke, P. Thomas,* phys. stat. sol. 41, 743 (1970).

[78] *F. Herman, J. P. Van Dyke,* Phys. Rev. Lett. 21, 1575 (1968).

[79] *P. LLoyd,* J. Phys. C 2 (1969).

[80] *K. Maschke, P. Thomas,* phys. stat. sol. 39, 453 (1970).

[81] *S. F. Edwards,* Proc. Roy. Soc. 167, 518 (1962).

[82] *S. F. Edwards,* Adv. in Phys. 16, 359 (1967).

[83] *S. Kirkpatrick,* Int. Conf. Am. Liqu. Semicond., Aug. 1971, Ann Arbour (Mich.) to be published in J. Non-Cryst. Sol.

[84] *I. N. Economu* and *M. H. Cohen,* Phys. Rev. Lett. 25, 1445 (1970).

[85] *F. Herman, R. L. Kortum, C. D. Kuglin* and *J. L. Shay,* Proc. Int. Conf. II–VI Semicond. Brown University 1967 ed. D. G. Thomas (Benjamin N.Y. 1968), 503.

[86] *D. Brust,* Phys. Rev. 186, 768 (1969).

[87] *D. Brust,* Phys. Rev. Lett. 23, 1232 (1969).

[88] *I. B. Ortenburger, W. E. Rudge, F. Herman,* Int. Conf. Am Liqu. Semicond., Aug. 1971, Ann Arbour (Mich.) to be published in J. Non-Cryst. Sol.

[89] *W. M. Hartmann* and *S. D. Mahanti,* Int. Conf. Am. Liqu. Semicond., Aug. 1971, Ann Arbour (Mich.) to be published in J. Non-Cryst. Sol.

[90] *V. L. Bonch-Bruevich,* phys. stat. sol. 42, 35 (1970).

[91] *J. Dow* and *J. J. Hopfield,* Int. Conf. Am. Liqu. Semicond., Aug. 1971, Ann Arbour (Mich.) to be published in J. Non-Cryst. Sol.

[92] *J. Sak,* private communication, to be published

[93] *K. Maschke,* phys. stat. sol. (b) 47, 511 (1971).

[94] *D. Beaglehole* and *M. Zavetova,* J. Non-Cryst. Sol. 4, 272 (1970).

[95] *R. Sandrock,* Phys. Rev. 169, 642 (1968).

[96] *A. G. Leiga,* J. appl. Phys. 39, 2149 (1968)
J. Opt. Soc. Amer. 58, 880 (1968).